LBL-19323
Preprint c.2

Lawrence Berkeley Laboratory
UNIVERSITY OF CALIFORNIA
Physics Division

Submitted to The Astrophysical Journal

NEW 33 GHz MEASUREMENTS OF THE COSMIC BACKGROUND RADIATION INTENSITY

G. De Amici, G. Smoot, S.D. Friedman,
and C. Witebsky

March 1985

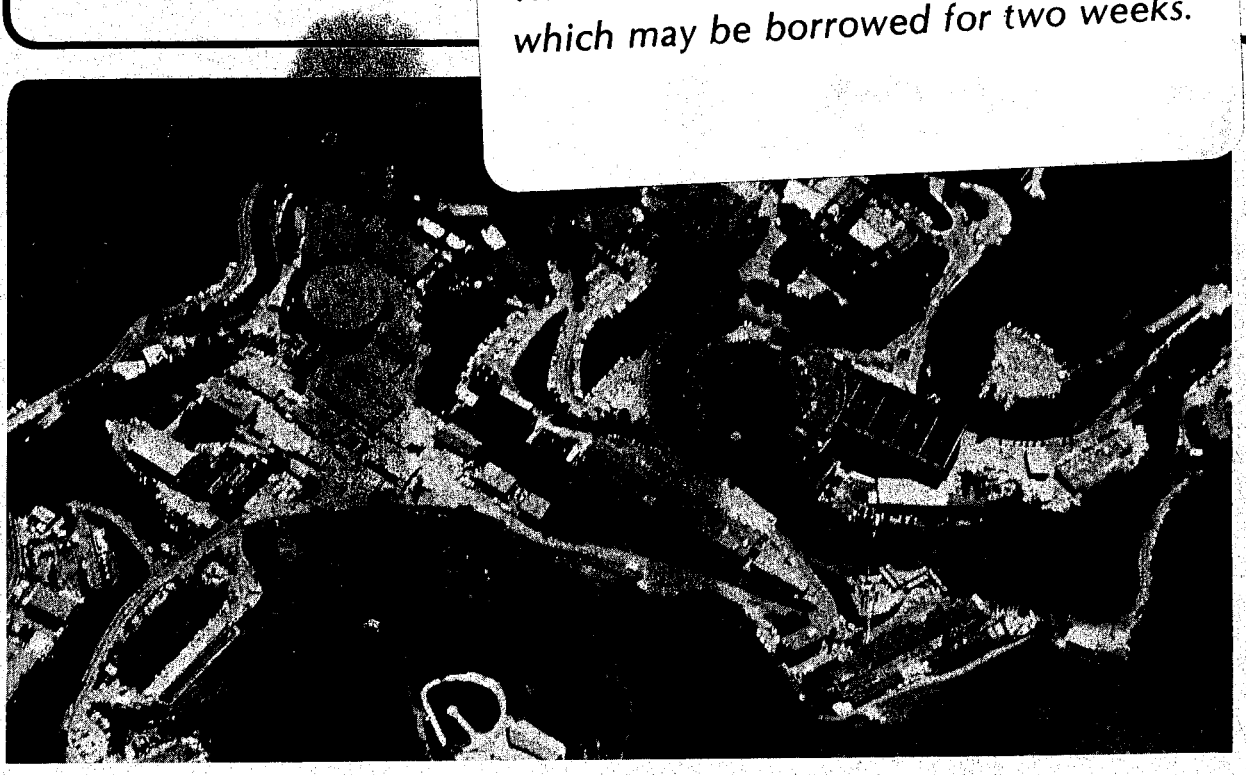

Prepared for the U.S. Department of Energy under Contract DE-AC03-76SF00098

NEW 33 GHz MEASUREMENTS OF THE COSMIC BACKGROUND RADIATION INTENSITY

Giovanni De Amici,[1] George Smoot, Scott D. Friedman,[2] and Chris Witebsky
Space Sciences and Lawrence Berkeley Laboratories
University of California, Berkeley

ABSTRACT

New measurements have been made of the intensity of the cosmic background radiation (CBR) at 33 GHz (0.91 cm). The experiment was part of a larger effort to measure the spectrum of the CBR between 2.5 and 90 GHz (12 and 0.33 cm). Details are given of the experimental equipment and measurement procedures. The results of measurements made in 1982 and 1983 are presented and discussed in relation to preliminary results from the other radiometers. The measured value, $T_{CBR} = (2.81 \pm 0.12)$ K, is in very good agreement both with those previously published and those reported by our collaborators.

I. INTRODUCTION

a) The Cosmic Background Radiation

The discovery of the cosmic background radiation (CBR) (Penzias and Wilson 1965) is considered by many to be the most important development in observational cosmology since the formulation of Hubble's law. Immediately interpreted as the relic radiation from an early, hot, dense phase of the universe (Dicke *et al.* 1965), the CBR has provided a tool to test competitive cosmological theories (Peebles 1971; Weinberg 1972; Steigman 1978) and put constraints on cosmological models and processes before the epoch of recombination. Its detailed structure (shape of the spectrum, polarization, anisotropy) is the only available probe into the very early universe ($z > 1500$).

Early observers measured the temperature of the background radiation in the low frequency (Rayleigh-Jeans) region to verify that the intensity spectrum followed a blackbody distribution. The importance of detecting the turndown (Wien region) of the spectrum soon shifted the region of the observations from low frequencies ($\nu < 40$ GHz) to the peak region ($\nu > 90$ GHz). Several excellent review papers (Weiss 1980; Thaddeus 1972; Wilkinson 1980) discuss the early measurements and their significance.

b) Reasons for Expecting Spectral Distortions

According to standard Big Bang cosmologies, the CBR should contain the footprints of the density fluctuations in the mass distribution from which the galaxies evolved (Weinberg 1972). Many attempts have been made to detect anisotropies in the CBR, on scales ranging from a few arcseconds to the full sky (Partridge 1980). Until now, however, the only anisotropies detected are those due either to the motion of the Earth with respect to the CBR (Gorenstein and Smoot 1981), or to Compton scattering of the photons by intergalactic gas (Birkinshaw *et al.* 1981). The failure to detect anisotropies has prompted speculation on possible processes taking place in the recent universe, that could have cancelled the records of a far past (Longair 1971). However, any process that could reheat the intergalactic gas and homogenize the CBR must leave a distinct mark on the spectrum of the CBR (Sunyaev 1974; Danese and De Zotti 1979). Positive detection of a deviation from a Planckian spectrum would provide information on the thermal history of the universe that might explain the negative results of anisotropy searches.

---

[1]Now at the Instituto di Radioastronomia CNR, Bologna, Italy

[2]Now at the University of California, San Diego.

The origin of galaxies should also leave an imprint on the CBR spectrum as well as producing anisotropies. For example, if galaxies originate as the result of accretion of matter moving in turbulent or whirlpool fashion, the scattered photons of the CBR would have a changed spectral distribution (Jones 1977; Bontz *et al.* 1981). Similarly, adiabatic fluctuations leading to galaxy formation will cause spectral distortions as well as anisotropies (Silk 1968). Any release of energy in the early universe will result in spectral distortion of the CBR. The spectral distortion parameters reveal the density of the universe, the expansion epoch during which the energy was released, and, possibly also the mechanism of energy release (Sunyaev and Zeldovich 1970).

c) Drawbacks of the Old Experimental Data

Evidence for a spectral distortion was announced by Woody and Richards (1981), who used a balloon-borne far-infrared spectrometer to measure the spectrum of the CBR in the range 71.5 GHz $< \nu <$ 400 GHz, near and beyond the peak of intensity.

As theoretical analysis has shown, the high frequency data alone are not sufficient to choose among the different possible scenarios (Danese and De Zotti 1979). Unfortunately, no measurement of the low frequency spectrum of the CBR of comparable precision was available at that time. All the measurements of the Rayleigh-Jeans spectrum had been performed before 1968 and, as Zeldovich *et al.* (1972) pointed out, they did not exclude the possibility of deviations from a blackbody spectrum as large as 15%.

The previous low frequency measurements were all made independently of one another. A few of them were carried out from the same location: the White Mountain Research Station's Barcroft Laboratory (Welch *et al.* 1967; Stokes *et al.* 1967; Wilkinson 1967; Ewing *et al.* 1967), but, except for the measurements by Stokes and by Wilkinson, no two measurements were ever made simultaneously. Most of them had different, if not contradictory, assumptions about the atmospheric emission. A large fraction had an atmospheric correction at least as large as the measured CBR temperature. Often, because of high system-noise temperatures, the experimenters were forced to integrate for extended periods of time, thus limiting the accuracy of the measurements because of the temporal variations of atmospheric emission.

II. THE INTERNATIONAL COLLABORATION

By the late 1970's the need for new, more accurate measurements of the low frequency part of the Cosmic Background Radiation spectrum was clear (Jones 1980). A collaboration was formed for the purpose of measuring the temperature of the CBR in the Rayleigh-Jeans part of the spectrum with a precision better than 5% and with a high relative accuracy in order to be very sensitive to spectral distortions. Members in the joint project were: the Istituto Fisica Cosmica C.N.R. of Milano, Italy responsible for the lowest frequency (2.5 GHz) radiometer (Sironi *et al.* 1984); the Istituto TESRE C.N.R. of Bologna, Italy with the 5 GHz receiver (Mandolesi *et al.* 1984); Haverford College of Haverford (Pennsylvania) with an atmosphere monitoring instrument at 9.4 GHz (Partridge *et al.* 1984); and the University of California at Berkeley which supplied the cold load calibrator (Smoot *et al.* 1983) and radiometers at 10 GHz (Friedman *et al.* 1984), at 33 GHz (DeAmici *et al.* 1984), and at 90 GHz (Witebsky 1985). The 33 and 90 GHz radiometers span the frequency gap between the Rayleigh-Jeans region and the submillimeter data obtained by Woody and Richards. The Osservatorio Astronomico dell' Universitá di Padova gave support in theory and atmospheric modelling.

To improve the relative accuracy of the measurements, they were all made at the same time from the same location and used the same large liquid-helium-filled cold-load calibrator (Figure 1). This device is described in Appendix A and by Smoot *et al.* (1983). In order to use the cold load, the radiometers have to be positioned on top of it. To make this movement as easy as possible,

each instrument is mounted on a cart that can be rolled along a 20-meter stretch of rails laid in the East-West direction. The cold load, located in the center of the rails, is suspended from the rails in a hole in the ground.

This paper describes the operations of and the results obtained from the 33 GHz receiver for measurements made in 1982 and 1983.

III. EXPERIMENTAL CONCEPTS

In order to measure the temperature of the CBR, it is first necessary to measure the total antenna temperature [1] of the sky at the zenith (T_{zenith}), which is the sum of contributions from the CBR ($T_{A.CBR}$), the atmosphere ($T_{A.atm}$), other celestial sources, such as the galaxy (T_{galaxy}), the Moon or the planets, and finally thermal emission from the ground entering the antenna sidelobes (T_{ground}):

$$T_{zenith} = T_{A.CBR} + T_{A.atm} + T_{galaxy} + T_{ground} \,. \tag{1}$$

Careful design of the equipment, proper choice of the experimental site and the time of the observations reduce the last two terms of equation (1) to negligible levels; T_{zenith} is measured and $T_{A.atm}$ can be inferred from models of the atmosphere and/or measured in real time (see also Section IV and Appendix B) by observing the intensity of atmospheric emission at various angles to the zenith.

T_{zenith} is obtained by measuring the difference in the output voltage when the radiometer looks at the zenith and when it looks at a reference load whose temperature is known. Adding the antenna temperature of the reference load yields the zenith temperature.

$$T_{zenith} = g(V_{zenith} - V_{load}) + T_{A.load} \,. \tag{2}$$

The calibration constant, g, discussed in detail in Appendix C is measured by pointing the radiometer at two targets whose temperatures are accurately known. Ideally they consist of two blackbody targets at widely different temperatures; we use the cold load calibrator and an ambient temperature load.

IV. THE 33 GHz RADIOMETER

a) General Description

The 33 GHz system consists of a receiver, support electronics, two oppositely-pointed corrugated-horn antennas, two flat mirrors, and the recording system (Figure 2). Everything but the data recording and power systems, which were shared with the other Berkeley radiometers, is

[1] Antenna temperature is defined as the temperature that, in the Rayleigh-Jeans approximation, would produce the received power over the instrument bandwidth:

$$P = kT_A B \,,$$

where T_A is the antenna temperature, P is the received power, B is the bandwidth and k is the Boltzmann's constant. It is related to the thermodynamic temperature, T, of the load according to:

$$T_A = \frac{x}{e^x - 1} T \,,$$

with $x = h\nu/kT$, where h is the Planck's constant, and ν is the frequency.

At long wavelengths, $x << 1$ and the antenna temperature is essentially equal to the thermodynamic temperature. At 33 GHz, x = 1.58/T; for temperatures of a few (3-4) K, the difference between T and T_A is as large as 20%.

mounted on the cart, so that it can be positioned over the cold load calibrator. The support electronics box is rigidly fixed to the cart. The receiver is mounted on bearings which allow it to rotate in a vertical plane perpendicular to the rails, and can be secured in either a vertical or horizontal position. Mounted on the north and south ends of the cart are two flat metallic mirrors. When the receiver is in the horizontal position, the mirrors intercept almost 100% of the antenna beam pattern. Tilting the mirror to an angle δ from horizontal allows the antenna to receive radiation coming from an angle $\theta = 90° - 2\delta$ from the zenith. The receiver is a standard superheterodyne radiometer, in a Dicke configuration (Kraus 1966) with the two input ports of the switch connected to two antennas.

The antennas are two conical horns, 35 cm long and with an aperture 12 cm in diameter. The internal walls of the horn are corrugated to increase the directivity and reduce the sidelobes (Lawrie and Peters 1966). The half-power beamwidth of the horns has been measured to be 7.5° (Figure 3) with an integral contribution from the first 30° of the beam pattern of more than 99.9% of the total signal received from an isotropic source (Janssen *et al.* 1979).

The Dicke switch is a magnetically driven ferrite circulator, operating at 100 Hz. Its insertion loss is 0.3 dB. The switch provides 23 dB isolation to the signal travelling in the backward direction. An isolator placed between the switch and the mixer reduces the local-oscillator-emitted power travelling from the mixer toward the switch and the horns.

The local oscillator generates a strong, constant signal at 32.91 GHz that is mixed with the signal received from the horns. The resulting signal at the difference frequency is fed to a first amplifier which provides 23 dB of power gain, and then to a second amplifier, which supplies additional power gain of 30 dB. A 3 dB attenuator located between the amplifiers helps to match the impedances and reduces signal reflections between the two amplifiers. The signal is finally rectified by a detector diode within the second amplifier's housing.

All the components from the horns to the detector diode are housed inside a 78 cm-long aluminum pipe, with the horns looking out the two open ends. The electronic components fit in the hollow space between the horns and the pipe's inner wall. This arrangement gives good rigidity to the assembly and provides excellent protection against mechanical shocks and stresses. Since the inner diameter of the pipe matches the outer diameter of the horn mouths, the pipe provided a very good shield against radio frequency interference. Magnetic shielding around the Dicke switch was provided by a layer of mu-metal foil.

The output voltage from the detector is carried, via a shielded cable, to a synchronous (lock-in) amplifier located in the electronics box. The lock-in detects the Dicke-modulated signal, amplifies it and integrates it for a 2-second period. Finally the analog signal is digitized and stored on magnetic cassette tape for later analysis.

Both the pipe and the box are thermally insulated with a 5 cm-thick layer of styrofoam. A thermostatic system, consisting of several power resistors controlled by temperature-monitoring circuits, keeps the electronic components at a fixed, stable temperature. The resistors can dissipate up to 18 watts sufficient to maintain the receiver at a constant temperature of 14°C under normal conditions. Because of the power dissipated by the electronics the temperature inside the box stays at a much higher value (25°C). The temperature inside the pipe and the electronics box is measured continuously by four temperature sensors in order to monitor temperature changes, which could affect the gain of the radiometer.

The warm load consists of a microwave absorber (an array of cast ferrite cones embedded in styrofoam) kept at ambient temperature. The reflectivity of the warm absorber has been measured to be less than −36.6 dB (0.02%) at 33 GHz; it therefore provides a very good blackbody target. The warm load is mounted in an insulated box to isolate it from air currents and other rapid temperature changes. Those changes that do occur are very smooth and gradual. Its temperature

Year	1982	1983
reflectors' nominal zenith angles	$+40°, +30°, -30°, -40°$ (North reflector)	$+50°, +45°, +40°, -35°, -40°$ (North reflector)
(+ means angle toward North − means angle toward South)	$-40°, -30°, +30°, +40°$ (South reflector)	$-50°, -45°, -40°, +35°, +40°$ (South reflector)
radiometer gain	14.8 ± 0.04 mK/du	9.52 ± 0.017 mK/du

Table 1: Differences between 1982 and 1983 instruments; the gain is quoted in mK/digitized unit (du), where a digitized unit is counts of ADC output.

is continually monitored and recorded via a sensor, accurate to $\pm 0.3°$C mounted inside the box in thermal contact with the absorber.

b) Advantages and Disadvantages in the Design

The advantage of having the horns looking in opposite directions is that the movements of the radiometer are kept to a minimum; the pipe remains stationary during measurements of the vertical atmosphere temperature (zenith scans) since the mirrors tilt to deflect the antenna beam to the appropriate angles, and only one movement (from horizontal to vertical position) is required to calibrate the radiometer or to measure the sky's zenith temperature. An additional advantage is that the horns' polarization plane does not rotate with respect to the mirrors' surfaces.

The design is not ideal, however, because it requires the pointing angle of the mirror to be known with great precision (1 arcmin of uncertainty in the angle introduces a 10 mK uncertainty in the vertical atmosphere temperature, and therefore in the cosmic background). Furthermore, the power actually reaching the radiometer includes a component emitted by the mirror itself, equal to the product of the mirror's temperature and its emissivity. The emissivity of the aluminum mirror is on the order of 10^{-4} and varies with the polarization of the incoming radiation and the incidence angle. To minimize the change in emissivity as a function of the angle of the mirror from the horizontal (Figure 4), we have rotated the antenna polarization plane by 30° with respect to vertical. The residual effect has been considered during the analysis of the data and will be further discussed in that context.

c) Modifications Between the 1982 and 1983 Systems

No major changes were made in the system design between the 1982 and 1983 measurements. Some aspects of the apparatus that needed improvement were identified and some minor flaws in the design were corrected (Table 1).

The single most important change was the replacement of the mirrors. In 1982 each mirror consisted of two 0.8 mm aluminum sheets glued to a 2.5 cm-thick sheet of plastic foam. Aluminum channels glued and bolted around the edges provided additional stiffness. When exposed to the temperature changes typical of the high altitude experimental site (during the daytime the sun-exposed part of the mirrors reached temperatures above 30°C, only to drop below −5°C during the night), the aluminum and plastic separated, and warps developed on the surface. In 1983, the

original mirrors were replaced by new ones made from an aluminum honeycomb core sandwiched between two flat aluminum sheets with aluminum channels glued all along the sides. The new mirrors performed admirably, and no subsequent problem ever arose.

The pointing system for the mirrors was also modified; in 1982, we estimated that the precision (repeatability) of the pointing was not better than 10 arcminutes; in 1983, we measured the repeatability to be within 2 arcminutes from the actual setting. The maximum zenith angle observed during atmospheric measurements was increased to 50°. Observations this far from the zenith reduced the uncertainty caused by pointing errors and thereby improved the quality of our measurements of the atmospheric antenna temperature. Table 2 provides a summary of the pointing situation during both years.

A new set of ground screens was used during the 1983 measurements. They were designed to intercept all of the antenna beam at angles within 20° of the axis (i.e. 99.8% of the total solid angle) even when the mirrors were tilted to deflect the beam to 50° from zenith.

The system gain was increased 40% (the calibration constant was decreased from 14.8 to 9.52 mK/du) to take full advantage of the dynamic range of the analog-to-digital converter and reduce any quantization problem arising from the digitization process. The full-scale limit of the amplification and detection chain was reduced to 310 K, where the maximum input was approximately 280 K.

V. CAUSES OF ERRORS IN MEASURING T_{CBR}

Both instrumental and external sources contribute to the background noise from which T_{CBR} must be extracted. This section discusses the sources of error that we considered while designing the instrument. Other effects, which became evident during operation will be discussed in the section describing the analysis of the data.

a) Instrument-Generated Background

The instrumental background is caused by the random thermal noise of the electronics components (switch, mixer, amplifiers). The receiver's noise temperature is approximately 800 K; this value is higher than what could be obtained with state-of-the-art instrumentation, but it is nevertheless at least an order of magnitude lower than the system noise of any receiver previously used for spectrum measurements in the 30 GHz frequency range (Puzanov *et al.* 1968; Welch *et al.* 1967; Wilkinson 1967; Ewing *et al.* 1967).

b) Natural Background

The natural background is due to thermal emission from the ground and the atmosphere, and thermal and synchrotron emission from celestial objects and the galaxy. The ground can be viewed as a warm (~ 280 K) blackbody source. The best way to account for the ground radiation is to prevent it from reaching the instrument. To do so, we erected a system of ground shields, consisting of metal sheets and wire screens, that act as mirrors causing the antenna to see sky rather than ground in its sidelobes.

Atmospheric emission is large (about 13 K at sea level under optimal conditions) and depends on the column density of both oxygen and water (Ulaby *et al.* 1981; Partridge *et al.* 1984). It varies with time, weather conditions, and location. The atmosphere also attenuates the CBR. We accounted for both effects by measuring the opacity of the atmosphere when we were measuring the CBR. The algorithm used to calculate $T_{A,atm}$ from the atmospheric measurements is discussed in Appendix B.

Other sources of natural radio background are the galaxy, the Sun, the Moon and the planets. Diffuse galactic emission is very weak at 33 GHz (less than 2 mK), and point sources like

	Nominal	Actual	Difference
1982 North reflector	0.0	+0.90	0.90 ± 0.17
	+40.0	+40.40	0.40 ± 0.17
	+30.0	+29.83	0.17 ± 0.17
	−40.0	−39.10	0.50 ± 0.17
	−30.0	−29.63	0.37 ± 0.17
1982 South reflector	0.0	−0.83	0.83 ± 0.17
	+40.0	+38.50	1.50 ± 0.17
	+30.0	+28.37	1.63 ± 0.17
	−40.0	−41.67	1.67 ± 0.17
	−30.0	−31.33	1.33 ± 0.17
1983 North reflector	0.0	+ 0.97	0.97 ± 0.03
	+50.0	+50.67	0.67 ± 0.03
	+45.0	+45.63	0.63 ± 0.03
	+40.0	+41.30	1.30 ± 0.03
	−35.0	−34.37	0.63 ± 0.03
	−40.0	−39.40	0.60 ± 0.03
1983 South reflector	0.0	+0.07	0.07 ± 0.03
	−50.0	−51.17	1.17 ± 0.03
	−45.0	−44.67	0.33 ± 0.03
	−40.0	−39.53	0.47 ± 0.03
	+35.0	+35.40	0.40 ± 0.03
	+40.0	+40.23	0.23 ± 0.03

Table 2: Nominal and real pointing angles (in degrees)

Reference	Frequency (GHz)	$T_{A,atm}$ (K)
Ewing *et al.* 1967	32.5	3.84 – 5.59
This Work	33.0	3.76 – 4.85
Wilkinson 1967	35.0	5.71 – 7.48

Table 3: Summary of atmospheric measurements near 33 GHz made from White Mountain Research Station at Barcroft

the planets do not contribute significantly to the total brightness of a 7.5° antenna beam. Nighttime observations assure that the Sun does not affect the measurements. The Moon also is a potential source of unwanted noise; care was taken to make measurements while the moon was far from the beam.

c) Design Techniques To Reduce the Effect of Noise

The effects of an 800 K noise temperature is reduced by using a Dicke-switched receiver. In such an instrument the output voltage is a linear function of the temperature difference between the two sources. The receiver is switched between the sources so rapidly (switching frequencies of many tens of Hertz are usual) that neither the system noise nor the gain can change significantly during a switching period (Kraus 1966; Evans and McLeish 1977). The system noise, together with bandwidth and integration time, determines the sensitivity of the receiver. The minimum temperature difference that our receiver could detect is 80 mK/sec$^{1/2}$. An 80 mK uncertainty is unacceptably large, so the receiver's digitized output is averaged for 32 seconds, resulting in a sensitivity of 15 mK.

d) Procedural Techniques to Reduce the Effect of Noise

The intensity of the atmospheric emission at 3800 m elevation is almost a factor of three lower than at sea-level. Even so, the atmosphere dominates the sky brightness. Previous experiments (Ewing *et al.* 1967; Wilkinson 1967) have measured atmospheric temperatures of about 5 K (Table 3). Regrettably there is no theoretical model that allows us to compute the vertical atmosphere temperature from other measurements with sufficient reliability and precision (Table 4 shows that the water vapor content, as measured by different instruments, yields only an order-of-magnitude agreement).

We therefore decided to measure the atmospheric emission directly. Since for a homogeneous atmosphere, the optical depth is a function of the atmospheric column density, it is sufficient to measure the difference in antenna atmospheric temperature at two or more zenith angles and then extrapolate to the emission at the zenith (App. B). Figure 5 shows the difference between values measured at zenith angle θ and the vertical. It is important to use the same instrument to measure both the atmospheric emission and the zenith sky brightness, because this procedure reduces the overall error due to uncertainty in the calibration of the instrument. As we will show later, if δg is the fractional error in the calibration, then the error in the measurement of T_{CMBR} is

Date	Radiometer				Optical
	9.4 GHz	10 GHz	33 GHz	90 GHz	Taken at sunset
1982 July 3			.46–.80	.60–.96	
1982 July 5	0.–.10	.15–.77	.30–.49	.43–.59	
1982 July 6	0.–.03	.15–.74	.30–.44	.43–.73	
1982 July 7	.17–.39		.49–.97	.62–1.15	
1983 Sept 3	.08		.25–.32	.31–.42	.23
1983 Sept 4	0.–.42	.09–.64	.11–.29	.18–.25	.20
1983 Sept 5	0.–.40	.09–.63	.20–.31	.26–.32	.27
1983 Sept 6	0.–.58	.17–.85	.31–.42	.32–.40	.38
1983 Sept 7	.24	.04–.44	.31–.50	.33–.40	

Table 4: Atmospheric water vapor content (g/cm^2) An optical device was used to measure the atmospheric water vapor content during the day. It was dependent upon sunlight for operations and could not be used during the actual data taking operations.

only δg times the temperature difference between the cold load and the CBR; in this experiment that difference is about 1 K.

VI. TESTS IN BERKELEY

Even though the instrument was designed to minimize the number of movements during operation, some movements could not be avoided: the cart had to be moved along the rails at least twice per night and the receiver had to be rotated from horizontal to vertical position every time the CBR was measured. Any of these movements could induce appreciable changes in performance. The instrument was tested in Berkeley to make sure that it was working properly to determine whether changes in external environment affected its behavior, and to measure its operating characteristics. The numerical results of the tests are summarized in Table 5.

Rotating the radiometer changes the orientation of the magnetically sensitive ferrite switch with respect to the earth's magnetic field, which can change the switch properties. We tested for this phenomenon by inducing a 10-gauss field in the space occupied by the radiometer. The direction of the field was periodically reversed. The tests were performed three times, with the field parallel to each axis of the radiometer. The first set of tests showed that a small (about 2 mK/gauss) effect was present; the switch was then wrapped with a layer of mu-metal. When the tests were repeated, the effect was negligible (0.3 ± 0.7 mK/gauss).

Rotating the radiometer also induced changes in the mechanical stresses on the different waveguide components. These in turn could alter the radiometric properties of the circuit, introducing a position-dependent change in the offset of the system. The ideal way to measure this behavior was to move the receiver through its positions while keeping stable cold loads over the horns. Unfortunately no load cold and stable enough to allow such a measurement was available. Instead we measured this effect by alternately pointing one antenna at two identical positions in the

Kind of test	Berkeley	White Mountain	Comment
magnetic	1 mK/gauss	not repeated	maximum output change
flip offset	< 10 mK	60 mK	offset change for 60 degree flip
sidelobes;			contribution to
side of mirror	< 1 mK	< 1 mK	signal from
bottom of mirror	< 1 mK	< 1 mK	sidelobes
top of mirror	230 mK	400 mK	and diffraction;
top of screen	50 mK	10 mK	worst case
integration	256 sec	512 sec	integration time
	4.7 mK	3.0 mK	minimum rms
Gain stability on 17 minutes test	0.3 %	0.2 %	peak-to-peak signal variation

Table 5: Results of the tests performed on the 33 GHz system

sky (i.e. at the same angle from zenith) while the second antenna looked at an ambient temperature load. The radiometer was then rotated and the tests repeated. These tests in Berkeley failed to show any effect above the system noise (< 10 mK).

Integration tests are designed to determine the time-averaged properties of the system noise. Modulations in the power supplied to the amplifiers, temperature drifts, and ground loops can all cause time-dependent variations in the output voltage. During an integration test, both antennas view the zenith sky and the output of the radiometer is recorded for 17 to 68 minutes. The data are then averaged over periods of 2^n seconds for successively larger values of n; if the fluctuations in the radiometer output consist solely of white noise, the r.m.s. variation in the resulting averages should decrease as $2^{-n/2}$. In Berkeley, the atmospheric noise becomes non-random for integration periods of about 64 seconds (corresponding to 13 mK r.m.s.) in normal conditions. This level is low enough that the uncertainty introduced in the measurement of the CBR is negligible when compared to other errors. One can evaluate the noise spectrum of the data by computing its Fourier transform and autocorrelation function; neither test gives any indication of periodic structure.

It is desirable that the radiometer gain stay constant over extended stretches of time. This feature is not critical, since our data-taking routine calls for calibrations every few minutes, but a constant gain is a convenient gauge of proper operation of the system and simplifies data analysis. The stability of the gain is better tested when the input loads are at widely different temperatures, so that a small gain change induces a large output-voltage change. We use an ambient-temperature load (about 290 K) and the zenith sky (about 15 K) as loads. The tests are made during calm, clear nights, so that no sudden variation in atmospheric emission, like that due to a passing cloud, could mimic a gain change. The gain change is computed taking the maximum and minimum values in the receiver output; the size of point-to-point fluctuations (90–100 mK) is indistinguishable from

the fluctuations due to sky variability. Over any 17-minute period the calibration never changed by more than 0.1% (0.2% in 1982).

The measured antenna pattern and simple geometrical considerations indicate that the reflectors and the screens intercept at least 99.8% of the beam, regardless of the position of the mirror. The ground around the receiver is so far from the antenna axis ($> 60°$) that it contributes less than 5 mK to the total signal. We could, however, have a detectable effect if stray radiation was diffracted around the screens and reached the receiver. We tested for this possibility by chopping an auxiliary screen in and out the possible path of the diffracted rays. No modulation (< 1 mK) was seen on the sides or the bottom part of the mirror. As expected, an effect (50 mK) was detected for the upper edge of the mirror, since it is much closer to the beam axis, so an auxiliary screen was added. Practical considerations limited the dimensions of this screen, so that a reduced (10 mK) effect was still measured during later tests. This was accounted for during the analysis of the data.

The frequency passband of the amplifiers (50–500 MHz) encompasses frequency channels commonly used for communication and broadcast. If these signals enter the amplification and detection chain, they can overwhelm the signal received by the antennas. The receiver is entirely enclosed in a metal case and all power and signal-carrying cables are shielded.

A test was conducted by broadcasting a modulated signal from close range. The frequency of the signal was swept across the passband of the amplifiers. The output of the receiver did not show any modulation (< 1 mK) which could be linked to the broadcast signal.

VII. DATA-TAKING IN THE FIELD

a) The Observation Site and Schedule

The measurements were performed at the Bancroft Laboratory of the White Mountain Research Station near Bishop California. This site is located on a mountain plateau at an altitude of 3800 meters above sea level, in an area where the atmospheric conditions are favorable for radiometric measurements during much of the year. The major drawback of the station is that access with heavy equipment is limited to the summer months (June – October) because of the usually heavy winter snowfall. On the other hand, its remote location reduces the amount of man-made radio-frequency interference to negligible levels (below the 5 mK threshold of detection) (Smoot 1984).

The actual time spent taking data amounted to only two nights (July 5 and 6, U.T.) in 1982 and to three nights (September 4, 5 and 6 U.T.) in 1983.

b) Tests, Controls and Practice Runs

Some of the tests described previously were repeated at the site. We tested again for gain stability, integration and flip offset. Since the horizon profile is different at White Mountain than in Berkeley, we also repeated the sidelobe measurements. The results of these second set of tests are reported in Table 5.

On the nights of 1982 July 3 and 7, 1983 August 30 and September 2 and 7, we put LN in the cold load and made practice runs. During all the nights of reasonably good weather, we made measurements of the vertical atmosphere temperature.

Radiometer position	Quantity measured	Target at: Blue horn	Target at: Red horn	Duration	Notes
1) vertical	T_{CBR}	cold load	zenith sky	64 sec	radiometer flipped halfway through
2) vertical	gain	cold load	warm load	64 sec	radiometer flipped halfway through
3) horizontal	offset	zenith sky	zenith sky	32 sec	
4) horizontal	$T_{A,atm}$	zenith sky	angle scan	32 N sec	N is the number of angles in the scan
5) horizontal	$T_{A,atm}$	angle scan	zenith sky	32 M sec	M is the number of angles in the scan

Table 6: Typical measuring sequence. Measurements using the LHe-cooled load had, as a general rule, M=N=2 in 1983 and M=N=4 in 1982. During 1982 the time spent on each position was only 16 seconds. The angles observed during the atmospheric scans are listed in Table 2. Measurements that did not use the cold load did not have position 1), and the zenith sky was used as the cold load in position 2. For these measurements M=N=4 in 1982 and M=N=5 in 1983.

c) Data-Taking Routine

Each measurement of the CBR consisted of several measurements of different targets. Unlike the lower-frequency radiometers used in the experiment, the 33 GHz system did not have a primary and a reference horn. Every observation had to be repeated with both antennas, but offsetting this disadvantage was the root-two reduction in the statistical uncertainty in measurements made using this configuration compared to those obtained with a system using always the same antenna as reference.

A typical measuring sequence consisted of a set of observations designed to measure the following quantities:

a) the calibration constant of the radiometer $[g]$

b) the instrumental offset $[T_{off}]$

c) the antenna temperature of the vertical atmosphere $[T_{A,atm}]$

d) the brightness difference between the zenith sky and the cold load $[g(V_{zenith} - V_{load})]$.

Table 6 gives a concise overview of the typical sequence.

Since changes in $T_{A,atm}$ of a few hundred mK were not uncommon on a time scale of 15 minutes, and since the error on the value of the temperature of the vertical atmosphere, $T_{A,atm}$, directly contributes to the error on the temperature of the CBR, it was important to make the measurements of $T_{A,atm}$ and T_{CBR} in rapid succession. Therefore a part of the time over the cold load calibrator was spent making atmospheric measurements. It took about 5 minutes to complete a set of measurements of the CBR and atmosphere.

VIII. ANALYSIS OF THE DATA

The data collected were first processed in the field within the next 24 hours. This real-time analysis was intended to assure that nothing was evidently going wrong; it allowed us to identify a ground-loop problem on 1983 September 4 and solve it before the next set of observations, saving the data of two following nights. The data were reprocessed and reanalyzed more thoroughly in Berkeley to derive the final results.

a) General Approach to Data Analysis

The antenna temperature of the CBR is determined by solving the equation:

$$T_{A,CBR} = g(V_{zenith} - V_{load}) + T_{A,load} - T_{A,atm} - T_{ground} - T_{galaxy}. \tag{3}$$

Only the first three terms on the right of equation (3) are significant. Extrapolations from published maps and measurements at long wavelengths (Haslam 1982) and from the galactic scans made at 2.5 GHz during this experiment (Sironi *et al.* 1984) place an upper limit of 2 mK on the galactic emission at 33 GHz during our observation times.

The design of the instrument, and specifically of the antennas was aimed at keeping the sidelobes as small as possible. Calculations from the measured beam pattern and direct sidelobe measurements have shown that the emission from the ground, T_{ground}, does not contribute more than 1 mK to the detected signal when the horn points vertically.

We can then rewrite equation (3) as:

$$T_{A,CBR} = g(V_{zenith} - V_{load}) + T_{A,load} - T_{A,atm}. \tag{4}$$

Of the quantities on the right side of equation (4), only the signal difference $(V_{zenith} - V_{load})$ is known directly from the data. $T_{A,load}$ depends on the physical temperature of the liquid helium and on the transmission properties of the dewar (Appendix A discusses the determination of $T_{A,load}$ and the associated error). A complete description of the method we used to determine the antenna temperature of the atmosphere, $T_{A,atm}$, and the calibration constant, g, is given in Appendixes B and C.

As stated previously, the short-time-scale variability (up to 100 mK in 15 minutes) of the atmospheric emission suggests making frequent measurements of $T_{A,atm}$ as a way to average the atmospheric effects. Our data-taking procedure yields a set of at least 4 values of $T_{A,atm}$ for each run. These values are averaged and the average normalized to the full set of the atmospheric measurements (see Appendix B). The resulting value of $T_{A,atm}$ is then substituted in equation (4) with the rms of the atmospheric data used as a weighting coefficient for the computed value of $T_{A,CBR}$. Next, the values of $T_{A,CBR}$ obtained during a night's measurements are combined to form a weighted average. The outcome of this procedure is given in Table 7.

b) Error Analysis

During our analysis of the data, we separately kept track of the statistical and systematic errors so as to get the best possible estimate of the experimental uncertainty. Referring to equation (4), we can write the uncertainty on $T_{A,CBR}$ as the sum of many contributions:

$$\begin{aligned} dT_{A,CBR} = &\frac{dg}{g}[(T_{A,CBR} + T_{A,atm}) - T_{A,load}] + gd(V_{sky} - V_{load}) \\ &- d(T_{A,load}) - \frac{dg}{g}(T_{A,atm}) - d(T_{A,atm}) , \end{aligned} \tag{5}$$

from which we get:

Date	Time (U.T.)	$T_{A.atm}$ [K]	T_{CBR} [K]	Number of runs
1982 July 3	7:18–9:06; 10:54–11:25	5.23–6.39		
	average	5.98±0.37		
1982 July 5	2:52; 4:10–5:09	5.02–5.62		
	9:00–9:15	4.82–4.91		
	11:33–14:01	4.58–4.88		
	6:09–6:55	4.67–5.13	2.86±0.04	9
	9:48–10:46	4.67–4.94	2.78±0.05	12
	average	4.85±0.12	2.82±0.03	21
1982 July 6	7:00	5.16		
	12:35–13:09	4.63–4.95		
	8:22–8:54	4.86–5.06	2.72±0.06	7
	9:50–10:23	4.86–5.02	2.70±0.06	7
	average	4.94±0.07	2.71±0.04	14
1982 July 7	3:46–4:27; 6:17–8:04	5.33–7.01		
	average	5.87±0.48		
1983 September 3	2:39–3:10; 7:05–7:28	4.51–4.73		
	average	4.64±0.08		
1983 September 4	4:33–5:04	4.13–4.23		
	6:36–7:17	4.14–4.44		
	8:27–8:46	4.06–4.40		
	5:43–6:28	3.76–4.63	2.86±0.10	10
	11:07–11:54	4.00–4.49	2.50±0.34	6
	average	4.23±0.10	2.83±0.10	16
1983 September 5	3:52–4:16	4.14–4.55		
	12:26	4.32		
	4:31–5:17	4.34–4.46	2.87±0.06	9
	10:40–11:20	4.35–4.50	2.80±0.06	7
	11:46–12:26	4.34–4.42	2.80±0.04	8
	average	4.41±0.05	2.81±0.03	24
1983 September 6	7:06–8:20	4.56–4.71		
	4:52–5:34	4.47–4.85	2.79±0.07	8
	average	4.64±0.05	2.79±0.07	8
1983 September 7	5:03–5:26; 9:51–10:23; 11:22–11:29	4.69–5.11		
	average	4.98±0.14		

Table 7: Results of atmospheric and CBR measurements. The atmospheric temperature is given as the range of variation during measurement interval. The quoted errors are statistical only. For the nights of measurements with LHe in the dewar, the results have been divided in sets corresponding to different data-taking times. For all other nights, the results refer to the all night period. The last column refers to the number of runs over the LHe dewar.

Nature	Quantity	Amplitude
Errors on $T_{A,atm}$		
Statistical:	rms of data	30-100 mK
	difference between angles	100 mK
Systematic:	gain	50 mK
	atmospheric temperature	< 15 mK
	atmospheric depth	< 10 mK
	beam shape	< 50 mK
	sidelobes	0-10 mK
	pointing	120 mK
	mirror emissivity	60 mK
	total in quadrature	145 mK
Errors on T_{CBR}		
Statistical:	rms of data	40 mK
	from $T_{A,atm}$	100-145 mK
Systematic:	gain	25 mK
	cold load temperature	25 mK
	flipoffset	100 mK
	from $T_{A,atm}$	145 mK
	total in quadrature	180 mK

Table 8: Amplitude of the errors (1982)

$$S_{T_{A,CBR}}{}^2 = \left(\frac{S_y{}^2}{g^2}\right)(T_{A,CBR} - T_{A,load})^2 + g^2 S^2 (V_{sky} - V_{load}) + S_{T_{A,load}}{}^2 + S_{T_{A,atm}}{}^2 . \quad (6)$$

The first term comes from the uncertainty in the measure of the radiometer's calibration constant; the second term derives from the statistical uncertainty in the output of the receiver and in the measurement of the flip offset; the third term is the error in the temperature of the cold load; the fourth is the uncertainty in the measured temperature of the atmosphere. The value of these uncertainties can be assessed from theoretical estimates, actual experimental data, and computer simulations. In Appendices A and C we estimate the uncertainties associated with the temperature of the cold load and the calibration of our receiver. Tables 8 and 9 show our best estimates of the magnitude of the errors.

The receiver noise is the dominant factor in the second term of equation (6) and is counted twice, since it affects both the determination of the radiometer offset and of the actual signal received. Its magnitude was determined by simply taking the product of the 1 sigma error of the data and the instrument calibration. The incomplete knowledge of the flip offset, given by the product of the offset and the calibration constant, could modulate the received signal.

Nature	Quantity	Amplitude
Errors on $T_{A,atm}$		
Statistical:	rms of data	20-80 mK
	difference between angles	100 mK
Systematic:	gain	25 mK
	atmospheric temperature	< 15 mK
	atmospheric depth	< 10 mK
	beam shape	< 50 mK
	sidelobes	0-20 mK
	pointing	20 mK
	mirror emissivity	60 mK
	total in quadrature	90 mK
Errors on the $T_{i:BR}$		
Statistical:	rms of data	40 mK
	from $T_{A,atm}$	100-130 mK
Systematic:	gain	25 mK
	cold load temperature	10 mK
	flipoffset	30 mK
	from $T_{A,atm}$	80-90 mK
	corrections on $T_{A,atm}$	80 mK
	total in quadrature	130 mK

Table 9: Amplitude of the errors (1983)

The error in $T_{A.atm}$, unfortunately, cannot be treated as easily as the others since the equation used for determining $T_{A.atm}$ is not a simple one and its differentiation is analytically cumbersome. We preferred to identify the sources of error and substitute into the equation the 1 sigma deviations; we then take the difference as the error in $T_{A.atm}$. Using a simplified notation, we can write:

$$S_{T_{A.atm}}{}^2 = S(noise)^2 + S(angle)^2 + S(T_{atm})^2 + S(beam)^2 + S(sidelobes)^2 + S(mirror)^2 + S(height)^2 \ , \tag{7}$$

where:

$S_{T_{A.atm}}$ = error in the antenna temperature of the vertical atmosphere
$S(...)$ = difference between $T_{A.atm}$ computed with the average and the 1 sigma values for:
the rms system noise,
the reflectors pointing angles,
the temperature of the atmosphere,
the shape of the antenna beam,
the sidelobes contribution,
the mirrors emissivity, and
the atmospheric scale height.

The effect of calibration error is treated separately for $T_{A.CBR}$ because it is correlated with the error in $(V_{sky} - V_{load})$. It is included in the estimated measurement error of $T_{A.atm}$ quoted in Tables 8 and 9.

The errors in the measurements of $T_{A.atm}$ and $T_{A.CBR}$ can be divided into two groups: statistical errors and systematic errors. In the first set, we put all the effects whose average amplitude is expected to decrease as the number of data points increases. The second set encompasses effects whose average amplitude is independent of the number of measurements made. As will be shown, statistical errors have very little effect on the precision of the measurement and the uncertainty in our value of the $T_{A.CBR}$ is essentially due to systematic errors. The numerical values of the different errors are given in Tables 8 and 9.

System noise produces a spread in the voltage output for any given input temperature, no matter how stable it is. Integration tests show that the uncertainty decreases as $t^{-1/2}$ for integration periods of up to 8 minutes.

Looking at different zenith angles we expect our line of sight to cross different and uncorrelated sky areas. We expect therefore to measure slightly different optical thickness from time to time, and more so when clouds are present in the sky. To compensate, we took data at many zenith angles and averaged the results.

As shown in Appendix C, the uncertainty in the calibration constant is small (about 0.5%). Because of its origin (mainly from imperfect knowledge of the non-linear response of the receiver) its effect does not decrease when more measurements are taken. Since our instrument is a Dicke radiometer the error in the calibration only matters for the antenna temperature difference between the reference cold load and the target, while the effect of calibration error on the temperature of the atmosphere cancels out. Because $T_{A.load} \simeq 3.0$ K and $T_{A.CBR} \simeq 2.0$ K, the overall effect is small. This is the only systematic error in measuring the atmosphere that does not have any appreciable consequence on the uncertainty in $T_{A.CBR}$.

In our calculation we use a fixed value of 250 K for the mean atmospheric temperature. Because of changes in composition, wind, and seasonal and diurnal variations, this value could be in error by as much as 20 K. The resulting change in the value of $T_{A.atm}$ derived from the measurements is less than 15 mK.

In our atmospheric convolution, we use a measured beam pattern. It deviates from the ideal Gaussian beam by about 1% (in integral shape); the resulting uncertainty is less than 50 mK.

We have measured the contribution from the ground nearby to be less than 10 mK in the worst conditions (reflector tilted to the lowest position) in 1982 and 20 mK in 1983.

During the CBR measurements, we used only four out of ten possible positions for the reflectors. During measurements of the atmospheric emission before and after the CBR measurements, the average $T_{A,atm}$, obtained from these four positions, is about 2% cooler than the overall average. We have corrected for this effect, which might be due to imperfect understanding of the atmospheric emission or to other systematic errors (e.g. non-detected cart tilt), but we have also added the same amount to the systematic errors.

The pointing angle of the reflectors can be measured during tests with a precision of at least 1 arcmin, but the repeatability was not better than 2 arcmin at any position in 1983. This uncertainty introduces a possible error of up to 25 mK. Because the reflector angles were not measured during the actual zenith scans.

We computed the reflectivity of the mirrors assuming a pure metal and laboratory conditions (Lorrain and Corson 1970). Measurements the emissivity of aluminum alloy sheets yielded values about 20% higher than expected from theoretical calculations, which would imply an emission of 60 mK higher.

In our model of the atmosphere we used an exponential density profile with scale height of 8 km. Even allowing for a 50% error, $T_{A,atm}$ does not change by more than 10 mK.

All these errors contribute to the uncertainty of $T_{A,atm}$. It should be noted that the statistical errors dominate the uncertainty on the single measurement of the atmospheric temperature. They contribute over 100 mK out of a typical error of 135 mK, but their effect over a night of observations reduces to less than 40 mK, for an overall uncertainty of 100 mK.

Statistical errors in $T_{A,CBR}$ are caused by the sum of the statistical errors in $T_{A,atm}$ discussed above and the system noise temperature. The latter affects both the offset and the measurement, so that the actual amplitude of the error is $\sqrt{2}$ times the measured system noise. Integration tests shown that the uncertainty decreases as $t^{-1/2}$. For integration times of 30 seconds, it reduces to less than 20 mK on each single measurement.

Uncertainties in the radiometric temperature of the cold load and in the position-dependence of the radiometer offset both contribute to the overall error in $T_{A,CBR}$. Appendix A discusses the phenomena that can affect the actual temperature of the cold load. We estimate to know the value of $T_{A,load}$ to within 10 mK. A slight difference (30 ± 30 mK) was measured between the radiometer's offset in the horizontal and vertical positions. Since we did not have a convenient and easy way to measure the vertical offset during the data taking runs, we used the horizontal offset and corrected for the observed difference.

IX. RESULTS AND OVERALL ERRORS

a) Comparison of Water Vapor Content Data

The results of all the nights of observation are summarized in Table 7, and in Figures 6 and 7. A few comments should be made about the numbers given there before we can proceed further in the data analysis process. It is evident that the measured vertical atmosphere's antenna temperature varies appreciably not only from night to night but also during a single night. Using the theoretical approach described by Partridge *et al.* (1984), we can transform the temperature data into water-vapor-content data and correlate our measurements with the measurements made simultaneously by our collaborators. Table 4 shows the atmospheric water vapor content as measured at 9.4, 10, 33 and 90 GHz. It was obtained using the relations(Danese and DeZotti 1984):

$$T_{A.atm}(9.4\ \mathrm{GHz}) = 1.038 + 0.027W \quad (8)$$

$$T_{A.atm}(10\ \mathrm{GHz}) = 1.055 + 0.033W \quad (9)$$

$$T_{A.atm}(33\ \mathrm{GHz}) = 3.589 + 0.358W \quad (10)$$

$$T_{A.atm}(90\ \mathrm{GHz}) = 5.389 + 1.951W\ , \quad (11)$$

where W is the atmospheric water-vapor content in mm.

The results are in substantial agreement, even if in some cases the water vapor content measured with different instruments barely overlap. In Figures 6a and 6b, we represent $T_{A.atm}$ as measured with the 10 and 33 GHz radiometers, and $T_{A.atm}$ as measured at 90 and 33 GHz. Regrettably, only about 30 simultaneous measurements were made with all three radiometers. The data plotted in Figures 6a and 6b were collected at different times during the nights of 1983 September 2, 3, 4 and 7; a fraction of them refer to measurements done while using the cold load. The data points used in the plots for the 10 and the 90 GHz radiometer were not taken concurrently. Even if unevenly spread, the data show a correlation between the 33 and the 90 GHz results; a linear best fit gives:

$$T_{A.atm}(33\ \mathrm{GHz}) = 0.20\ T_{A.atm}(90\ \mathrm{GHz}) + 2.22\ \mathrm{K}\ , \quad (12)$$

compared to:

$$T_{A.atm}(33\ \mathrm{GHz}) = 0.18\ T_{A.atm}(90\ \mathrm{GHz}) + 2.6\ \mathrm{K}\ , \quad (13)$$

obtained from equations (10) and (11). The 10 GHz data, on the other hand, appear to be independent of the results from the other radiometers. It is clear that our understanding of the emission processes in the atmosphere and in the radiometers is far from being complete.

b) Criteria Used in Editing the Data

Although measurements of the CBR were made on consecutive nights (1982 July 5 and 6 U.T. and 1983 September 4, 5, and 6 U.T.), and the quality of the data obtained is not constant. Those taken on 1982 July 6 show an abnormally large spread in the atmospheric temperature measured at different zenith angles, while those recorded on 1983 September 4 are affected by an evident short-time-scale and position-dependent change in offset.

We believe that the problem on 1982 July 6, was caused by the deformation of the front surface of the mirrors, due to differential expansion of the materials used which severely affected the pointing angles of the mirrors and their flatness (De Amici *et al.* 1984). Even if the averages over each run are consistent with the data obtained by our collaborators at other frequencies and with this same instrument during previous nights, it is impossible to account for systematic differences of as many as 800 mK in the temperature of the vertical atmosphere measured at different zenith angles. In 1983 we experienced a ground loop problem; it was due to differences in the coupling between the instrument and the rail-cold load system when the radiometer was rotated in vertical position. This caused the offset to change by as much as 1.2 K (about 60% of its normal amount) even during a single run. The measurements of the atmosphere were not affected by this, but the results reported in Table 7 for T_{CBR} for the night of September 4, even if consistent with the outcome of the other nights, have very large statistical errors, resulting from an anomalous spread in the individual measurements. Because of these large errors, the data from July 6 and September 4 are not included in the analysis.

c) Combination of Different Errors and Final Results

The values of $T_{A,cBR}$ from each night of measurements were weighted by their statistical errors and averaged. The results of our measurements are presented in Figures 7, 8 and 9. The statistical errors in the averages (shown in Table 7) were added in quadrature to the systematic errors (discussed in Part V and listed in Tables 8 and 9), and the antenna temperatures were converted to thermodynamic temperatures to yield the values:

$$\text{1982 July 5} \qquad T_{cBR} = (2.82 \pm 0.21)\text{K} \tag{14}$$

$$\text{1983 September 5} \quad T_{cBR} = (2.81 \pm 0.14)\text{K} \tag{15}$$

$$\text{1983 September 6} \quad T_{cBR} = (2.79 \pm 0.15)\text{K} . \tag{16}$$

It should be noted that the value quoted here for 1982 July 5 is slightly different from the previously published one (Smoot *et al.* 1983). The analysis procedure previously used for the 1982 data has been described elsewhere (De Amici *et al.* 1984). The following considerations have led to minor changes in the analysis procedure:

a) Better measurements of the saturation effects in the radiometer have caused us to change our correction for the effective antenna temperature of the warm load, therefore inducing a change in the calibration of the instrument (see also Appendix C).

b) Computations of the atmospheric antenna temperature used a numerical convolution of the measured antenna beam pattern with the atmospheric distribution. Previously, the beam pattern had been modeled as a Gaussian.

c) As stated in Appendix A, we recomputed the radiometric properties of the cold load, specifically the contribution of the walls and of the interface between the horn and the dewar, under the assumption that it behaves like a cylindrical waveguide. Geometrical considerations of the properties of the antenna beam and measurements of cylindrical targets simulating the inner wall of the cold load, indicate that the outcome of the computation should be regarded as an upper limit only. This induces a small change in the radiometric temperature of the cold load, which affects the final result (1).

The combined effect of the changes in points a) and b) is to reduce the value of T_{cBR} by about 20 mK; the other 30 mK reduction comes from the temperature of the cold load.

We combine the 1983 results by averaging the values of T_{cBR} using the statistical errors (0.03 and 0.07) as weighting factors and adding the systematic errors to the final value. This yields for the 1983 data:

$$T_{cBR} = (2.81 \pm 0.14)\ \text{K}. \tag{17}$$

Combined with the 1982 result equation (14), which is treated as an independent measurement, it becomes:

$$T_{cBR} = (2.81 \pm 0.12)\ \text{K}. \tag{18}$$

d) Comparison with Previous Results

The previous measurements in the 33 GHz range were carried out fourteen years ago at frequencies of 35 GHz (Wilkinson, 1967), 32.5 GHz (Ewing *et al.* 1967) and 36.5 GHz (Puzanov *et al.* 1968 and Kislyakov *et al.* 1971). They reported:

$$T_{cBR} = (3.16 \pm 0.26) \quad \text{K} \quad \text{at } 32.5\,\text{GHz} \tag{19}$$

$$T_{cBR} = (2.56^{+0.17}_{-0.22}) \quad \text{K} \quad \text{at } 35\ \text{GHz} \tag{20}$$

$$T_{cBR} = (2.4 \pm 0.9) \quad \text{K} \quad \text{at } 36.5\,\text{GHz}. \tag{21}$$

Frequency [GHz]	CBR Temperature [K]
2.5	2.77 ± 0.13
4.75	2.70 ± 0.08
10.0	2.75 ± 0.11
33.0	2.81 ± 0.12
90.0	2.57 ± 0.14

Table 10: Combined results of 1982 and 1983 experiments

The weighted average of those measurements is:

$$T_{CBR} = 2.76 \pm 0.15 \text{ K} \tag{22}$$

This measurement is less than half a standard deviation from that value.

X. INTERPRETATION AND COMMENTS

a) Overall Results of the Experiment

The important feature of this experiment is that the measurements are made at multiple frequencies. Since the blackbody character of the CBR spectrum in the Rayleigh-Jeans region has been long established (Stokes *et al.* 1967), little can be learned from an isolated single frequency measurement. The cosmological significance of the 33 GHz result will therefore be discussed together with the results from the other instruments. The overall results, which have been published and discussed elsewhere (Smoot *et al.* 1983, 1984), have been repeated in Table 10 for clarity and convenience.

b) Summary of the Available Data

The weighted average of our five measurements is: (2.73 ± 0.05) K. It agrees very closely with the average, T_{CBR} = (2.74 ± 0.09) K, of all the previous low frequency ($73.5 \geq \lambda \geq 0.33$cm) experiments, but is in disagreement with the high frequency ($\lambda < 0.3$ cm) balloon data (Woody and Richards 1981). They reported a T_{CBR} ranging between 2.88 and 3.28 K, with typical errors of 0.10 K, in the frequency range between 71.5 and 400 GHz. Recent measurements in the peak region have been made using the transition lines of interstellar CN molecules (Meyer and Jura 1984). Excitation temperatures of (2.73 ± 0.04) K at 2.64 mm (113 GHz) and (2.8 ± 0.3) K at 1.32 mm (227 GHz) were found. These values, which should be considered as absolute upper limits on T_{CBR}, do not fit with the Woody and Richards' data, but are in excellent agreement with our results. The new measurements of Peterson, Richards and Timusk (1984) with a weighted average of 2.78 ± 0.11 K , are in agreement with our results. Figure 10 shows all the published low frequency measurements and the recent high frequency measurements of the CBR.

c) Theoretical Justification

It was shown (Illarionov and Sunyaev 1975) that for any mechanism of energy release into the primordial universe, the resulting distortion of the CBR spectrum can be described analytically with the same formulas used for the Compton scattering. The distorted spectrum has a Bose-Einstein distribution, with the occupation number n defined by the characteristic chemical potential μ:

$$n = \frac{1}{e^{(x+\mu)} - 1} , \tag{23}$$

where $x = h\nu/kT$. Since such a spectrum produces a higher temperature in the Wien region than in the Rayleigh-Jeans region, we expect it to yield a better fit to the Woody and Richards data and our data than a simple black-body spectrum.

Given enough time since the energy release, low energy photons created by bremsstrahlung raise the temperature at long wavelengths and recreate a Planckian distribution. Sunyaev and Zeldovich (1970); Danese and De Zotti (1980) have modeled the resulting spectrum with a frequency dependent chemical potential $\mu(x)$. Under the hypothesis of small deviations from a Planck distribution (which is surely true at the present time), the chemical potential can be written as:

$$\mu(x) = \mu_{\circ} e^{-x_1/x} , \tag{24}$$

where:

$$x_1 = 100\omega^{1/2} g(x)^{1/2} z^{-3/4} \tag{25}$$

$$\omega = (H_0/50 \text{ km/sec/Mpc})^2 \Omega. \tag{26}$$

The value of x_1 identifies the frequency where the Compton and bremsstrahlung processes balance each other. Above this frequency the spectrum has a Bose-Einstein distribution, below it is Planckian. The red shift z refers to the time the energy was released.

d) Fit of the Data to Distorted Spectra

Using the χ^2 test, we fit the data of Table 10 and Figure 8 to the spectrum of equation (23) using $\mu_{\circ}$ and T as variables. Minimizing the χ^2 gives the most likely values of the parameters. This yields :

$$\mu_{\circ} = (-1 \pm 3)10^{-3} \tag{27}$$

and

$$T = 2.71 \pm 0.08K, \tag{28}$$

with $\chi^2 = 1.97$ for 3 degrees of freedom for our data alone, and:

$$\mu_{\circ} = (-0.8 \pm 1.7)10^{-3} \tag{29}$$

and

$$T = 2.72 \pm 0.03K, \tag{30}$$

with $\chi^2 = 18$ for 26 degrees of freedom for all the measurements. For the other low frequency measurements, we used the values available in the literature (Danese and De Zotti 1978; Otoshi and Stelzried 1975). It is evident that the data do not support the hypothesis of a Bose-Einstein spectrum, but are rather consistent with a black-body distribution ($\mu = 0$).

Even allowing for the frequency dependence of equation (24), under reasonable values of ω and z the chemical potential $\mu_{\circ}$ is never larger than 10^{-2} either when we fit to the data from this experiment or when we use the whole body of low frequency measurements (Tables 11 and 12). The values assumed by $\mu_{\circ}$ in both cases are negative and are not statistically significant. Again these results suggest that the value of $\mu_{\circ}$ is consistent with zero which in turn indicates that the CBR has a blackbody spectrum.

	$z = 10^4$	$z = 10^5$	$z = 10^6$
$\omega = 1.0$			
μ_{ν}	$(-0.6 \pm 16.0)\ 10^{-3}$	$(-1.3 \pm 3.8)\ 10^{-3}$	$(-0.9 \pm 2.7)\ 10^{-3}$
T	2.69 ± 0.13	2.71 ± 0.08	2.71 ± 0.08
χ^2	1.95	1.97	1.97
$\omega = 0.1$			
μ_{ν}	$(-1.7 \pm 5.1)\ 10^{-3}$	$(-1.0 \pm 2.9)\ 10^{-3}$	$(-0.9 \pm 2.6)\ 10^{-3}$
T	2.70 ± 0.09	2.71 ± 0.08	2.71 ± 0.07
χ^2	1.97	1.97	1.97
$\omega = 0.01$			
μ_{ν}	$(-1.1 \pm 3.2)\ 10^{-3}$	$(-0.9 \pm 2.7)\ 10^{-3}$	$(-0.9 \pm 2.6)\ 10^{-3}$
T	2.71 ± 0.08	2.71 ± 0.08	2.71 ± 0.07
χ^2	1.97	1.97	1.97

Table 11: Best fits of measurements of T_{CBR} to a frequency dependent Bose-Einstein spectrum [weighted average of 1982 and 1983 results of this spectrum experiment only] Note: the χ^2 was computed for 3 degrees of freedom.

	$z = 10^4$	$z = 10^5$	$z = 10^6$
$\omega = 1.$			
$\mu_{..}$	$(-1.9 \pm 7.3)\ 10^{-3}$	$(-0.8 \pm 2.2)\ 10^{-3}$	$(-0.8 \pm 1.6)\ 10^{-3}$
T	2.72 ± 0.035	2.72 ± 0.03	2.72 ± 0.03
χ^2	18.2	18.2	18.0
$\omega = 0.1$			
$\mu_{..}$	$(-0.8 \pm 2.9)\ 10^{-3}$	$(-0.8 \pm 1.7)\ 10^{-3}$	$(-0.8 \pm 1.5)\ 10^{-3}$
T	2.72 ± 0.03	2.72 ± 0.03	2.72 ± 0.03
χ^2	18.2	18.0	17.9
$\omega = 0.01$			
$\mu_{..}$	$(-0.8 \pm 1.5)\ 10^{-3}$	$(-0.8 \pm 1.5)\ 10^{-3}$	$(-0.9 \pm 1.5)\ 10^{-3}$
T	2.72 ± 0.03	2.72 ± 0.3	2.72 ± 0.03
χ^2	18.0	18.0	17.9

Table 12: Best fits of measurements of T_{CBR} to a frequency dependent Bose-Einstein spectrum [all published measurements of T_{CBR}] Note: the χ^2 was computed for 26 degrees of freedom.

e) Theoretical Interpretation

Several authors (Sunyaev and Zeldovich 1970; Chan and Jones 1975; Illarionov and Sunyaev 1975; Danese and De Zotti 1980; Jones 1980) have discussed the constraints that the assignment of a well-defined value to μ would put on the evolutionary history of the universe. Neglecting phenomena which occurred during the first 10^{-35} seconds (dealt with by the inflationary theories), the evolution of the spectrum of the CBR can be divided into three periods, according to the effectiveness with which bremsstrahlung and Compton scattering can alter the CBR spectrum. These epochs are bounded by the redshifts z_{μ} and z_{h}, defined as:

$$z_{h} = 10^{5}\omega^{-6/5} \tag{31}$$

and

$$\begin{aligned} z_{\mu} &= 10^{4}\omega^{-1/5} \qquad \text{if } \omega > 0.6 \\ z_{\mu} &= 10^{4}\omega^{-1/2} \qquad \text{if } \omega < 0.6. \end{aligned} \tag{32}$$

During the first period ($z > z_{h}$) any distortion in the spectrum is smoothed out and erased by the combined action of Compton scattering and bremsstrahlung. Regardless of any process that might have occurred during this period, the resulting CBR spectrum is that of a black-body. During the second period ($z_{h} > z > z_{\mu}$), however, there is not enough time for the bremsstrahlung to regenerate the photons that are displaced to high energy as a result of energy release, and the equilibrium distribution is a Bose-Einstein spectrum. Finally, for $z < z_{\mu}$, not even Compton scattering is effective in creating a Bose-Einstein spectrum. A release of energy at this time will decrease the intensity in the Rayleigh-Jeans region, while conserving the shape of the spectrum, and enhance the intensity in the high frequency region.

If energy release occurred during the period $z_{h} > z > z_{\mu}$, the amount of energy released is related to the chemical potential μ_{o} by the relation:

$$\delta U/U_{o} = 0.7\mu_{o} \tag{33}$$

where: $\delta U = U_{r} - U_{o}$; U_{r} = energy density of the spectrum after the perturbation and; U_{o} = energy density of the unperturbed spectrum. The quantity $\delta U/U_{o}$ is related also to the maximum temperature deviation in the Rayleigh-Jeans spectrum:

$$\frac{\delta T_{A}}{T_{A.RJ}} = \frac{\delta U}{U_{o}}\frac{1}{2x_{1}} = \frac{\mu_{o}}{ex_{1}} \tag{34}$$

where $\delta T_{A} = T_{A.max} - T_{A.RJ}$; $T_{A.max}$= greatest deviation from a Planckian spectrum; $T_{A.RJ}$= Rayleigh-Jeans temperature. The frequency where this deviation occurs is defined by x_{1}; it is therefore dependent upon the time z of energy release, with limits: $x_{1} > 0.02\omega^{7/5}$ when $z < z_{h}$ and $x_{1} < 0.2\omega^{7/8}$ if $\omega < 0.6$ when $z \simeq z_{\mu}$, or $x_{1} < 0.2\omega^{13/20}$ if $\omega > 0.6$. Our limits on μ_{o} ($\mu_{o} < 10^{-2}$) and on δT_{A} ($\delta T_{A.max} < 0.1T_{A.RJ}$), set a constraint on x_{1}: $x_{1} < 4 \times 10^{-2}$ or $\nu_{i} < 2.4$ GHz. Precise measurements in this frequency range are very difficult to obtain, because of the amount of man-made radio noise and the presence of strong synchrotron emission from our galaxy, which dominates the signal from the CBR for frequencies lower than 1 GHz. Differential measurements can be performed (the Berkeley and Milano groups are studying a program for such an experiment), but the data available now (Howell and Shakeshaft 1966), do not permit any conclusion on the presence of a distortion. Of course, if the deviation is much smaller, it could fall in a more easily accessible frequency range, but then measurements with a increased sensitivity will be required.

If the release of energy happens at $z < z_{\mu}$, the CBR retains a black-body spectrum that is Comptonized (Illarionov and Sunyaev 1975). It is worth noting that the most accurate measurements in this region available to date (Meyer and Jura (1984) and Peterson, Richards and Timusk

(1984)) do not support this possibility. The parameter describing the Comptonization is:

$$u = \int \frac{k(T_e - T_r)}{m_e c^2} d\tau \tag{35}$$

where $d\tau = n_e \sigma_T \, dl$, k is Boltzmann's constant, T_e is the electron temperature, T_r is the radiation temperature in the Rayleigh-Jeans region, m_e is the electron rest mass, n_e is the electron number density, σ_T is the Thomson scattering cross-section, and l is the path length. The optical depth for Thomson scattering is τ, while $k(T_e - T_r)/m_e c^2$ is the mean fractional energy (frequency) shift per Thomson scattering. Thus u represents the effective Comptonization scattering optical depth. The best fitted values are $T_{e:BR} = 2.73 \pm 0.03$ K and $u = (-0.3 \pm 1.1) \times 10^{-2}$ providing an upper limit on u of 10^{-2} at the 68% confidence level.

This experiment could not have been done without the skilled help of many friends and colleagues whom we would like to thank: J. Aymon, A. Benner, P. Calzolari, H. Dougherty, G. Epstein, J. Gates, J. Gibson, N. Gusack, S. Levin, P. Lubin, E. Mattaini, F. Mitschang. The staff and crew of the White Mountain Research Station provided invaluable help during our field operations, well beyond their normal duties.

This work was supported by N.S.F. Grants No. PHY 80-15694 and AST 800737, by the Department of Energy under Contract DE-AC03-76SF00098. and by C.N.R. Fellowships nos. 203.2.13 and 203.2.15.

Source	Antenna Temperature [K]
LHe cooled Eccosorb	3.039 ± 0.004
Emission from windows	0.002 ± 0.001
Gas	negligible ($<< .001$)
Insertion losses from wall	0.005 ± 0.005
Reflection from load	0.008 ± 0.004
Reflection from windows	0.012 ± 0.002
Total	3.068 ± 0.008

Table 13: Antenna temperature at 33 GHz of the liquid-helium-cooled reference load

APPENDIX A
THE LHe COLD-LOAD CALIBRATOR

The precise knowledge of the antenna temperature of the cold load is essential for accurate measurements of the CBR. The cold load calibrator (Smoot *et al.* 1983) consists of a large (75 cm diameter, 150 cm deep) cylindrical metal cryostat (Figure 1). The inside of the cylinder is isolated from the ambient air by two 0.023 mm thick polyethylene windows. The boiled off helium gas from the cryostat is warmed in a heat exchanger and passed into the space between the polyethylene windows in order to prevent condensation of moisture on the windows. For radiometric purposes the inside of the cold load consists of a cylindrical wall of mylar, coated with 0.013 mm (27 skin depths at 33 GHz) of aluminum. The aluminum-coated wall acts like a 70 cm diameter oversized waveguide terminated with a 20-cm-thick slab of Eccosorb VHP-8, a carbon-loaded urethane foam with pyramidal points on its upper surface. This material is an almost perfect absorber at microwave frequencies and behaves like a blackbody for all practical purposes. The cold load has performed satisfactorily during both years and provided a cold, stable target.

The radiation reaching an antenna that looks into the cold load is the sum of several components whose values are reported in Table 13:

a) Thermal radiation from the target and the floor of the cold load depends on the physical temperature of the coolant, on the emissivity of the material and on the insertion loss of the transmission line. The temperature of the LHe was monitored continuously by a pressure gauge and two sensor diodes. The readings from both systems agree very well, but uncertainties in the driving current of the diodes limit their absolute precision to 20 mK. Conversely, the pressure gauge has a precision of 1 mm Hg; even allowing for uncertainties in the pressure added by the weight of the He gas inside the container, the error on the pressure measurements is equivalent to an uncertainty of 4 mK in LHe boiling temperature. This higher precision makes the pressure readings a better gauge of the boiling point of the LHe. During each year the temperature of the Eccosorb target stayed constant within 8 mK, the limit of our measurement sensitivity (Witebsky 1984).

Tests have shown that the transparency of the Eccosorb target at 3 GHz is less than 2.5×10^{-4}. Both the target and the stainless steel cryostat floor beneath it are maintained at a constant temperature by the boiling LHe.

b) Insertion losses from the walls and the calibrator-horn coupling depend on the physical temperature and the material of these components. Insertion loss from these components not only

attenuates the radiation from the Eccosorb, but it also adds a spurious component of its own:

$$T_{out} = T_{in} e^{-\tau} + T_{phys}(1 - e^{-\tau}) \qquad (A.1)$$

where τ is the insertion loss of the wall and coupling components.

Measurements have yielded low values (10^{-5}) for the insertion loss of the wall (De Amici 1984). These measured values have been used in the data analysis and are reported in Table 13.

c) Insertion losses from the windows have been measured by inserting many layers of material between the horn and a well know target. The temperature difference so obtained was used to estimate the contribution of a single layer under the linear hypothesis. The number of layers was then halved to check that no saturation effect was present.

d) Power leaking from the receiver to the horns and reflected back by the load can add a significant contribution to the apparent temperature of the load. For our radiometer, insertion losses in the switch and imperfect isolation between ports broadcast (40 ± 5) K into the calibrator. Most of this power is absorbed by the Eccosorb and only a small fraction is reflected back into the antenna. The measured reflectivity of the dry cold load at room temperature is less than −38 dB at 33 GHz, so its emissivity is greater than 0.9998. An upper limit of −26 dB reflectivity has been measured for the calibrator filled with liquid nitrogen—in this case the reflectivity is dominated by dielectric reflection at the gas-LN interface. Measurements made by our collaborators at different frequencies with liquid helium in the cold load suggest that the presence of liquid helium does not significantly alter the radiometric properties of the dry Eccosorb (De Amici 1984). More important is the reflection from the windows, whose value accounts for an additional 7 mK.

APPENDIX B
THE ATMOSPHERIC ANTENNA TEMPERATURE $T_{A.atm}$ AT VERTICAL

The antenna temperature of the zenith sky, as measured from the radiometer, is a complex function of many independent variables. Analytically, we can express the temperature observed at a given zenith angle θ as:

$$T(\theta) = T_{CBR}e^{-\tau(\theta)}R(\theta) + T_{atm}(1 - e^{-\tau(\theta)})R(\theta) + T_{refl}(1 - R(\theta)), \qquad (B.1)$$

where $R(\theta)$ is the reflectivity and T_{refl} is the ambient temperature of the aluminum mirror. The optical depth at an angle θ, $\tau(\theta)$, can be expressed as the optical depth at the zenith times the relative column density of the atmosphere:

$$\tau(\theta) = \tau(0)f(\theta). \qquad (B.2)$$

Near the zenith $f(\theta) \approx \sec(\theta)$ When θ becomes larger $f(\theta)$ should be expressed as:

$$f(\theta) = \sec(\theta) - (\sec(\theta)^3 S/2), \qquad (B.3)$$

where S is the ratio between the vertical scale depth of the atmosphere and the earth's radius. The difference between a flat slab and a curved atmosphere is never larger than a fraction of a percent.

At 33 GHz, the atmosphere is still very transparent ($\tau(\theta) << 1$), so we can expand the exponential in a series:

$$e^{-\tau(\theta)} = 1 - \tau(\theta) + \tau(\theta)^2/2 - \tau(\theta)^3/6. \qquad (B.4)$$

Since τ is of order 2×10^{-2}, the error introduced by neglecting terms of order $\tau(\theta)^4$ and higher is small. Equation (B.1) can be rewritten, using the above notation and remembering that our antennas have a beam of finite size, as:

$$\begin{aligned} T(\theta) = {} & T_{CBR}R(\theta)\left[1 - a(\theta)\tau(0) + b(\theta)\tau(0)^2/2 - c(\theta)\tau(0)^3/6\right] \\ & + T_{atm}R(\theta)\left[a(\theta)\tau(0) - b(\theta)\tau(0)^2/2 + c(\theta)\tau(0)^3/6\right] + T_{refl}[1 - R(\theta)] \end{aligned} \qquad (B.5)$$

with :

$$a(\theta) = \int f(\psi)g(\phi,\chi)d\phi d\chi$$

$$b(\theta) = \int f(\psi)^2 g(\phi,\chi)d\phi d\chi$$

$$c(\theta) = \int f(\psi)^3 g(\phi,\chi)d\phi d\chi$$

where :

θ = angle between the zenith and the center of the main lobe

ψ = angle between the zenith and the integration element

ϕ = angle between the center of the main lobe and the integration element

χ = rotation angle of the integration element around the center of the main lobe,

and

$$\cos(\psi) = -\sin(\chi)\cos(\phi)\sin(\theta) + \cos(\chi)\cos(\theta)\ .$$

Equation (B.5) can be rearranged in the form:

$$T(\theta) = R(\theta)\left\{T_{CBR} + (T_{atm} - T_{CBR})\left[a(\theta)\tau(0) - b(\theta)\tau(0)^2/2 + c(\theta)\tau(0)^3/6\right]\right\} + T_{refl}[1 - R(\theta)]\ . \qquad (B.6)$$

The difference between the temperature at the zenith and at the angle θ, can then be written as:

$$T(\theta) - T(0) = T_{c:BR}(R(\theta) - R(0)) + (T_{atm} - T_{c:BR})[A(\theta)\tau(0) - B(\theta)\tau(0)^2/2 + C(\theta)\tau(0)^3/6] + T_{refl}[R(0) - R(\theta)], \quad (B.7)$$

where:

$$A(\theta) = a(\theta)R(\theta) - a(0)R(0)$$
$$B(\theta) = b(\theta)R(\theta) - b(0)R(0)$$
$$C(\theta) = c(\theta)R(\theta) - c(0)R(0).$$

The left hand being nothing else than the output of the radiometer,

$$gV = T(\theta) - T(0),$$

we can define:

$$W \equiv gV + (T_{refl} - T_{c:BR})\frac{(R(\theta) - R(0))}{(T_{atm} - T_{c:BR})}, \quad (B.8)$$

and:

$$\epsilon \equiv W/A(\theta).$$

Equation (B.7) then becomes:

$$\epsilon = \tau(0) - \frac{1}{2}\frac{B(\theta)}{A(\theta)}\tau(0)^2 + \frac{1}{6}\frac{C(\theta)}{A(\theta)}\tau(0)^3. \quad (B.9)$$

Solving (B.9) for $\tau(0)$, and substituting into (B.6), after rewriting it for the zenith, we get:

$$T(0) = T_{c:BR}R(0) + T_{refl}[1 - R(0)] + (T_{atm} - T_{c:BR})R(0)\epsilon\left\{a(0) + \epsilon\left[a(0)\frac{B(\theta)}{2A(\theta)} - b(\theta)/2\right] + \epsilon^2\left[\frac{B(\theta)}{2A(\theta)}\left(a(0)\frac{B(\theta)}{A(\theta)} - b(0)\right) + \frac{1}{6}\left(c(0) - a(0)\frac{C(\theta)}{A(\theta)}\right)\right]\right\}. \quad (B.10)$$

Since we are interested in the temperature of the atmosphere at the zenith, when it is observed without a reflector, we can drop the first two terms on the left side of the [14] and the $R(\theta)$ factor in the third term:

$$T_{va} = (T_{atm} - T_{c:BR})\epsilon\left\{a(0) + \epsilon\left[a(0)\frac{B(\theta)}{2A(\theta)} - b(\theta)/2\right] + \epsilon^2\left[\frac{B(\theta)}{2A(\theta)}\left(a(0)\frac{B(\theta)}{A(\theta)} - b(0)\right) + \frac{1}{6}\left(c(0) - a(0)\frac{C(\theta)}{A(\theta)}\right)\right]\right\}. \quad (B.11)$$

We solved equation (B.11) for each atmospheric measurement and arranged the results in matrixes of 10 columns (1 for each pointing angle) by N rows, where N is the number of zenith scans during a given night. We noticed that the column averages tend to be randomly distributed, but the average over the 4 columns referring to the $+50°$ and $+40°$ angles for the north reflector and $-50°$ and $-40°$ angles for the south reflector yields a value which is usually about 2% lower than the overall average. This effect is present in the data recorded during all the nights and its amplitude ranges from 2.0 to 2.8%.

APPENDIX C
MEASURING THE RADIOMETER'S GAIN

The calibration constant, g, of the radiometer is the conversion coefficient between measured voltage output differences and input antenna temperature differences. To first order it is the ratio between the antenna temperature of a target that fills the antenna beam and the output voltage of the receiver:

$$g = \Delta T_{ant} / \Delta V_{out}. \qquad (C.1)$$

It is measured by pointing each horn alternately at two loads whose temperatures are widely different. It is common to use an ambient temperature load and a similar target at very low (often liquid nitrogen) temperature. We had the convenience of having available a liquid helium cooled load; the temperature baseline for gain calibration was therefore as large as 280 K. The temperature in the numerator of equation $C.1$ is then the difference in temperature of the two loads, and the denominator is the difference in the output voltages:

The corrections for the antenna temperature of the radiometer can be easily accounted for by computing the antenna temperature of the load. They are negligible for the ambient temperature load and became important only for LHe cooled loads. This definition is only an approximation, however, since it does not account for the fact that an instrumental offset is always present and that, for large input signals, the detection diode could present a more or less pronounced effect of nonlinearity.

We looked for saturation effects in the detecting diode, by applying higher and higher input power voltages. The test showed no evidence for diode saturation up to twice the input power levels typical of the experiment. A small saturation was detected in the data recorded during practice tests in Berkeley. We measured the magnitude of the effect by recording the output signal for four different input temperature loads: ambient (285 K) Eccosorb, dry ice (194 K) Eccosorb, liquid nitrogen (77 K) Eccosorb and the sky at the zenith during a clear, dry night in Berkeley (16 K). We then fit different polynomial curves (first and second order) to the experimental points and used the results to calculate the calibration constant of the radiometer.

The uncertainty in the temperature of the loads was typically 0.3 K except for the dry ice load, whose temperature, because of poor thermal contact between Eccosorb and coolant, is not known to better than 2 K.

For an ambient-temperature load the correction for saturation is less than about 1%; it is negligible for any load temperature below the LN_2 boiling point. The errors in the determination of the calibration constant come from uncertainties in the input temperatures, in uncertainties in the output readings V_{out}, and from an imperfect knowledge of the diode saturation. Table 14 reports numerical estimates for these effects: it is clear that the dominant factor is the uncertainty in the saturation correction. The overall uncertainty on the calibration constant of the receiver is less than 0.5%.

1982 Measurements		
Error	Amount	Gain error resulting [mK/du]
ambient temperature load	300 mK	1.7×10^{-2}
cold load	30 mK	9.6×10^{-4}
output voltages	3 du	2.4×10^{-3}
saturation correction	1 %	1.5×10^{-1}
Total:		1.6×10^{-1} mK/du
1983 Measurements		
Error	Amount	Gain error resulting [mK/du]
ambient temperature load	300 mK	6.9×10^{-3}
cold load	30 mK	3.8×10^{-4}
output voltages	3 du	1.2×10^{-3}
saturation correction	0.4 %	3.9×10^{-2}
Total:		4.2×10^{-2} mK/du

Table 14: Errors in determining the gain of the radiometer (du = digitized units)

APPENDIX D
EXPLANATIONS OF SYMBOLS

β	attenuation	[Nepers/m]
ϵ	emissivity	dimensionless
λ	wavelength	[cm]
μ	Bose-Einstein chemical potential	dimensionless
θ	angle from zenith	[degrees]
τ	optical depth	dimensionless
Ω	ratio of actual density to the critical density of the universe	dimensionless
B	radiometer bandwidth	[Hz]
f, F	frequency of interest	[Hz]
g	gain of the radiometer	[K/du]
$g(x)$	frequency dependent Gaunt factor	dimensionless
h	Planck's constant (6.626×10^{-27})	[erg-sec]
H_0	Hubble constant	[km/sec/Mpc]
k	Boltzmann's constant (1.380×10^{-16})	[erg/K]
n	photon occupation number	
P	power received by the radiometer	[watt]
T	thermodynamic temperature	[K]
T_A	antenna temperature	[K]
$T_{A,atm}$	antenna temperature of the atmosphere	[K]
$T_{A,CBR}$	antenna temperature of the CBR	[K]
$T_{A,load}$	antenna temperature of the cold load	[K]
T_{atm}	physical temperature of the atmosphere	[K]
T_{CBR}	thermodynamic temperature of the CBR	[K]
T_{gal}	galactic emission	[K]
T_{ground}	contribution from sidelobes (mostly ground emission)	[K]
T_{in}	input temperature	[K]
T_{out}	output temperature	[K]
T_{refl}	physical temperature of the reflector (usually ambient temperature)	[K]
$T_{A,atm}$	radiometric (antenna) temperature of the atmosphere at the zenith	[K]
V_{off}	instrument's offset	[du]
x	normalized frequency ($h\nu/kT$)	dimensionless
z	red shift	dimensionless

REFERENCES

Birkenshaw, M., Gull, S. F., and Northover, K. J. E. 1981, *Mon. Not. R. Astr. Soc.,* **197**, 571.

Barlow, H. E. M. 1947, *Microwaves and Waveguides* (London: Constable).

Bontz, R. J., Price, R. H., and Haugan, M. P. 1981, *Ap. J.,* **246**, 592.

Chan, K. L., and Jones, B. J. T. 1975, *Ap. J.,* **195**, 1.

Danese, L., and De Zotti, G. 1978, *Astron. Astroph.,* **68**, 157.

Danese, L., and De Zotti, G. 1980, *Astron. Astroph.,* **84**, 364.

Danese, L., and De Zotti, G. 1984, *private communication.*

De Amici, G., et al. 1984, *Phys. Rev. D,* **29**, 2677.

De Amici, G. 1984, *Astrophysical Note* **445**.

Dicke, R. H., et al. 1965, *Ap. J.,* **142**, 414.

Evans, G., and McLeish, C. W. 1977, *RF Radiometer Handbook* (Dedham: Artech House).

Ewing, M. S., Burke, B. F., and Staelin, D. H. 1967, *Phys. Rev. Lett.,* **19**, 1251.

Friedman, S. D. 1984, *Ph. D. Thesis,* University of California, Berkeley, and *Lawrence Berkeley Laboratory Report* **LBL-17279.**

Friedman, S. D., et al. 1984, *Phys. Rev. D.,* **29**, 2677.

Gorenstein, M. V. and Smoot, G. F. 1981, *Ap. J.* **244**, 361.

Haslam, C. G. T., et al. 1982, *Astron. Astroph. Suppl. Ser.,* **47**, 1.

Howell, T. F., and Shakeshaft, J. F. 1967, *Nature,* **210**, 1318.

Illarionov, A. F., and Sunyaev, R. A. 1975, *Soviet Astron.,* **18**, 691.

Janssen, M. A., et al. 1979, *IEEE Trans. Ant. Prop.,* **AP27**, 551.

Jones, B. J. T. 1977, *Mon. Not. R. Astr. Soc.,* **180**, 151.

Jones, B. J. T. 1980, *Physica Scripta,* **21**, 732.

Kraus, J. D. 1966, *Radioastronomy* (New York: McGraw-Hill).

Kislyakov, A. G., et al. 1979, *Sov. Astr. AJ,* **15**, 29.

Laurie, R. E., and Peters, L. 1966, *IEEE Trans. Ant. Prop.,* **AP14**, 605.

Longair, M. S. 1971, *Rep. Progr. Phys.,* **34**, 1125.

Lorrain, P., and Corson, D. R. 1970, *Electromagnetic Fields and Waves* (San Francisco: Freeman and Co.).

Mandolesi, N., et al. 1984, *Phys. Rev. D,* **29**, 2680.

Meyer, D. M., and Jura, M. 1984, *Ap. J. Lett.,* **276**, L1.

Otoshi, T. Y., Stelzried, C. T. 1975, *IEEE Trans. on Instruments and Measurement*, **24**, 174.

Partridge, R. B. 1980, *Physica Scripta,* **21**, 624.

Partridge, R. B., et al. 1984, *Phys. Rev. D.,* **29**, 2683.

Peebles, P. J. E. 1971, *Physical Cosmology* (Princeton: Princeton University Press).

Peterson, J. B., Richards, P. L., and Timusk, T. 1984, *Submitted P.R.L.*.

Penzias, A. A., and Wilson, R. W. 1965, *Ap. J.,* **142**, 419.

Puzanov, V. I., Salomonovich, A. E., and Stankevich, K. S. 1968, *Sov. Phys. Astronomy,* **11**, 905.

Silk, J., 1968, *Ap. J.,* **151**, 459.

Sironi, G., et al. 1984, *Phys. Rev. D,* **29**, 2986.

Smoot, G., et al. 1983, *Phys. Rev. Lett.,* **51**, 1099.

Smoot, G., et al. 1985, *Ap. J. Lett.*.

Steigman, G. 1978, *Ap. J.,* **221**, 407.

Stokes, R. A., Partridge, R. B., and Wilkinson, D. T. 1967, *Phys. Rev. Lett.,* **19**, 1199.

Sunyaev, R. A., and Zeldovich, Y. B. 1970, *Astroph. Sp. Sc.,* **7**, 20.

Sunyaev, R. A. 1974, in *Proc. 63rd IAU Symposium,* ed. M. Longair (Dordrecht: Reidel), p. 167.

Thaddeus, P. 1972, *Annual Rev. Astron. Astroph.,* **10**, 305.

Ulaby, F. T., Moore, R. K., and Fung, A. K. 1981, *Microwave Remote Sensing* (Reading: Addison-Wesley).

Weinberg, S. 1972, *Gravitation and Cosmology* (New York: Wiley and Sons).

Weiss, R. 1980, *Annual Rev. Astron. Astroph.,* **18**, 489.

Welch, W. J., et al. 1967, *Phys. Rev. Lett.,* **18**, 1068.

Wilkinson, D. T. 1967, *Phys. Rev. Lett.,* **19**, 1195.

Wilkinson, D. T. 1980, *Phys. Scr.,* **21**, 606.

Witebsky, C. 1985, *Ph. D. Thesis,* University of California, Berkeley, and *Lawrence Berkeley Laboratory Report* **LBL-18746.**

Witebsky, C. 1984, *Astrophysical Note* **444.**

Woody, P., and Richards, P. 1981, *Ap. J.*, **248**, 18.

Zeldovich, Y. B., Illarionov, A. F., and Sunyaev, R. A. 1972, *Sov. Phys. JETP,* **35**, 643.

This work was supported by the U.S. Department of Energy under Contract No. AC03-76SF00098.

GIOVANNI DE AMICI: Instituto di Radioastronomia CNR, via Irnerio 46, 40126 Bologna, Italy

GEORGE SMOOT, and CHRIS WITEBSKY: 50/232 Lawrence Berkeley Laboratory, University of California, Berkeley, CA 94720

SCOTT FRIEDMAN: CASS C-011; UC San Diego; La Jolla, CA 92093

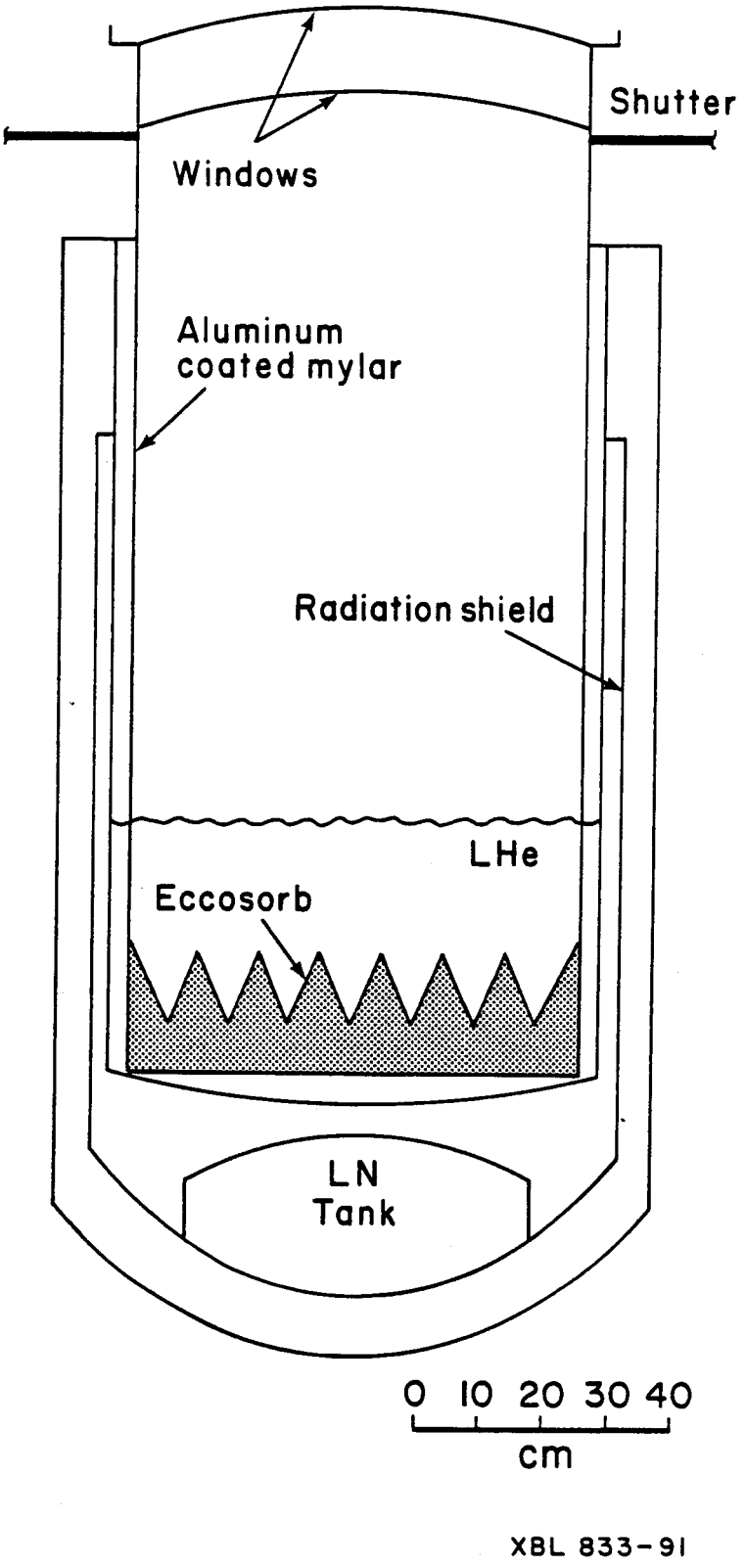

Figure 1 - Schematic representation of the liquid-helium-cooled calibrator, showing the elements determining the radiometeric performance of the load.

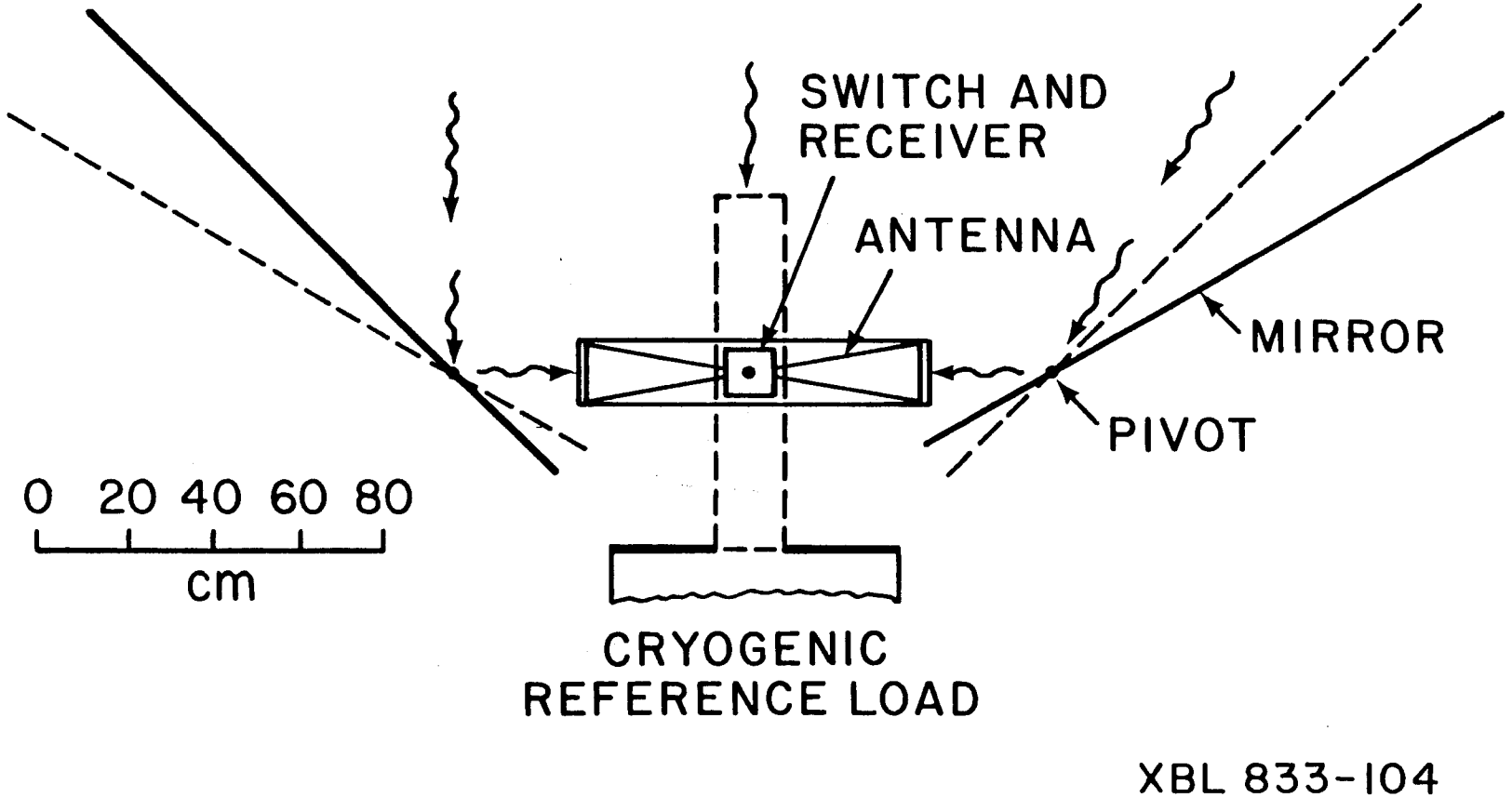

Figure 2 - Schematic representation of the 33 GHz radiometer showing the operation of mirrors

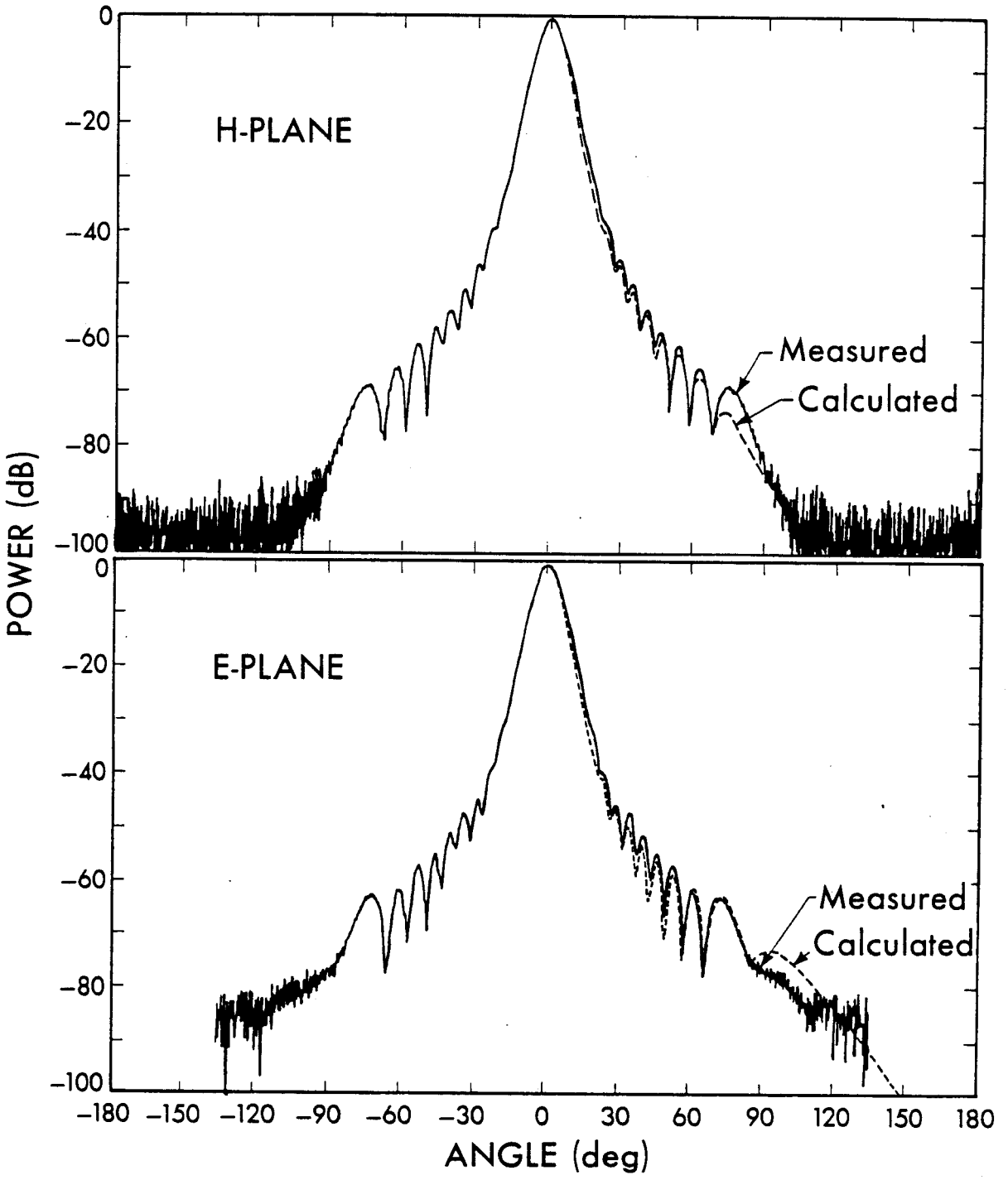

Figure 3 - Antenna beam pattern for the conical corrugated horns. a) E-plane radiation pattern; b) H-plane radiation pattern: — measured - - - calculated. (Janssen *et al.* 1979).

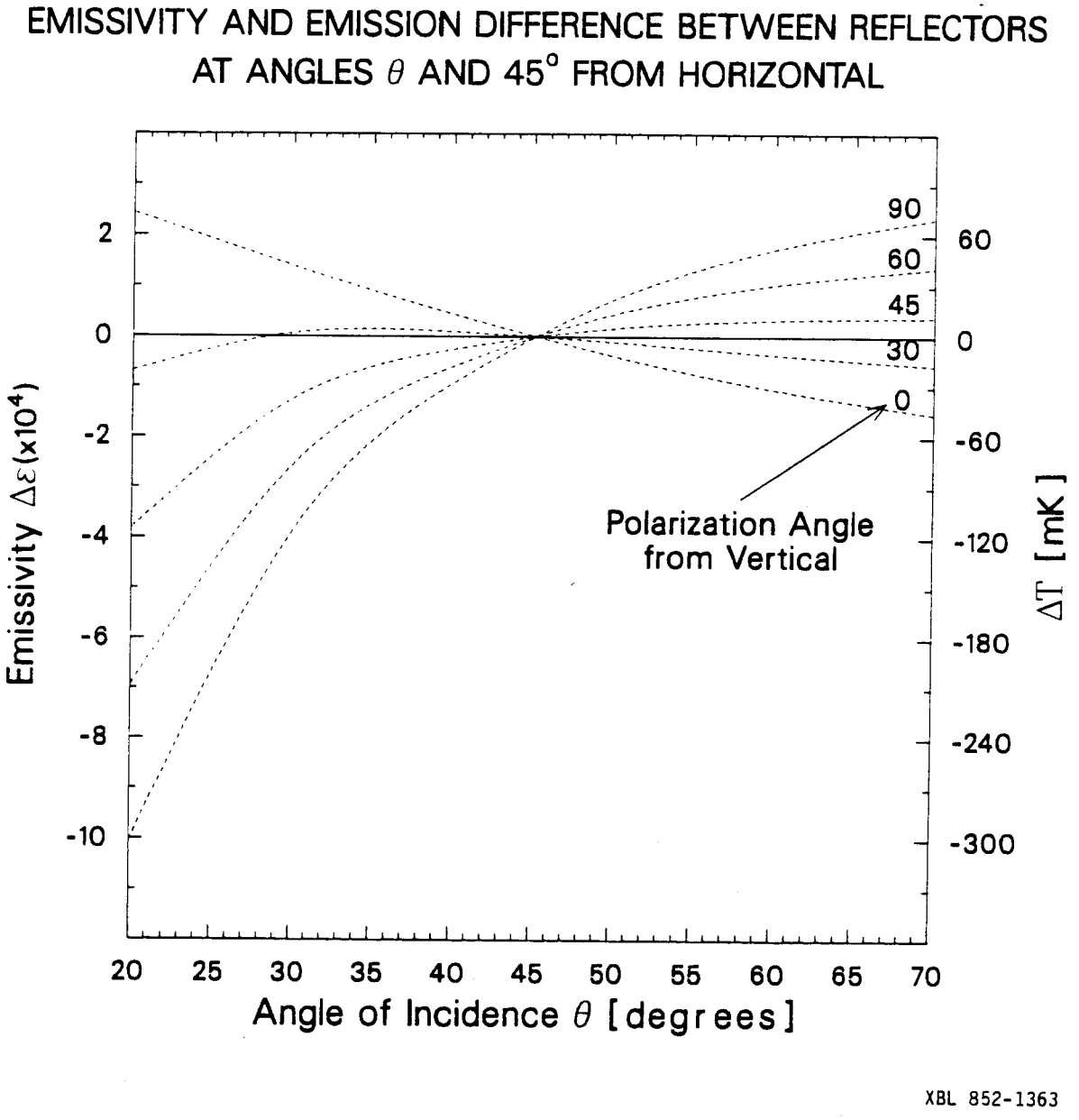

Figure 4 - Emissivity and emission difference between reflectors at angles θ and at 45° from horizontal; the polarization angle of the waveguide (angle from vertical) is a free parameter and is indicated for each curve.

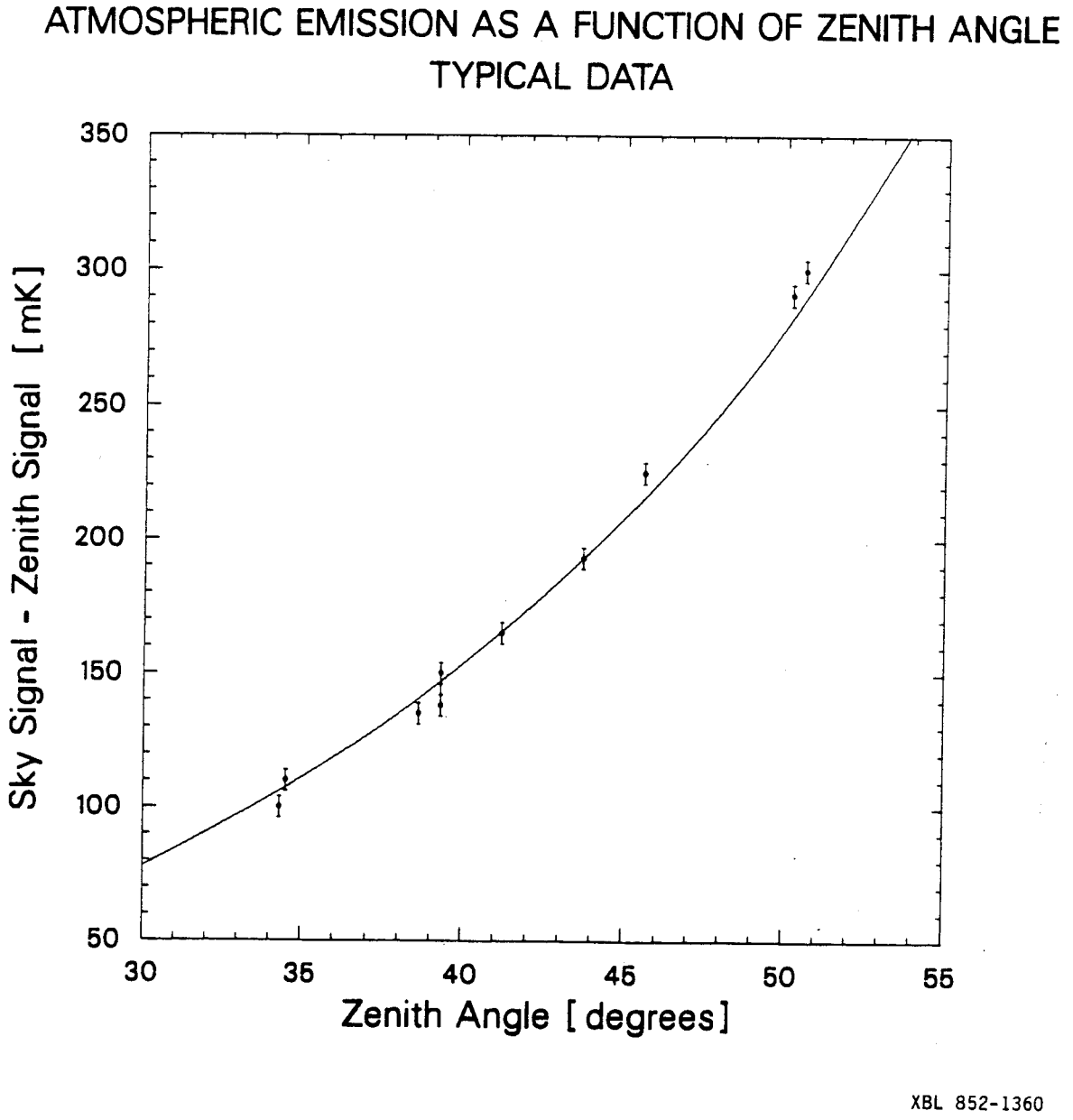

Figure 5 - Atmospheric emission versus zenith angle. The points are the difference between the measured value at angle θ and the zenith. The curve, added to aid the eye, is (sec $\theta - 1$) scaled by $T_{A,atm}$. a) Typical values for a single run. b) Values average for one nights data.

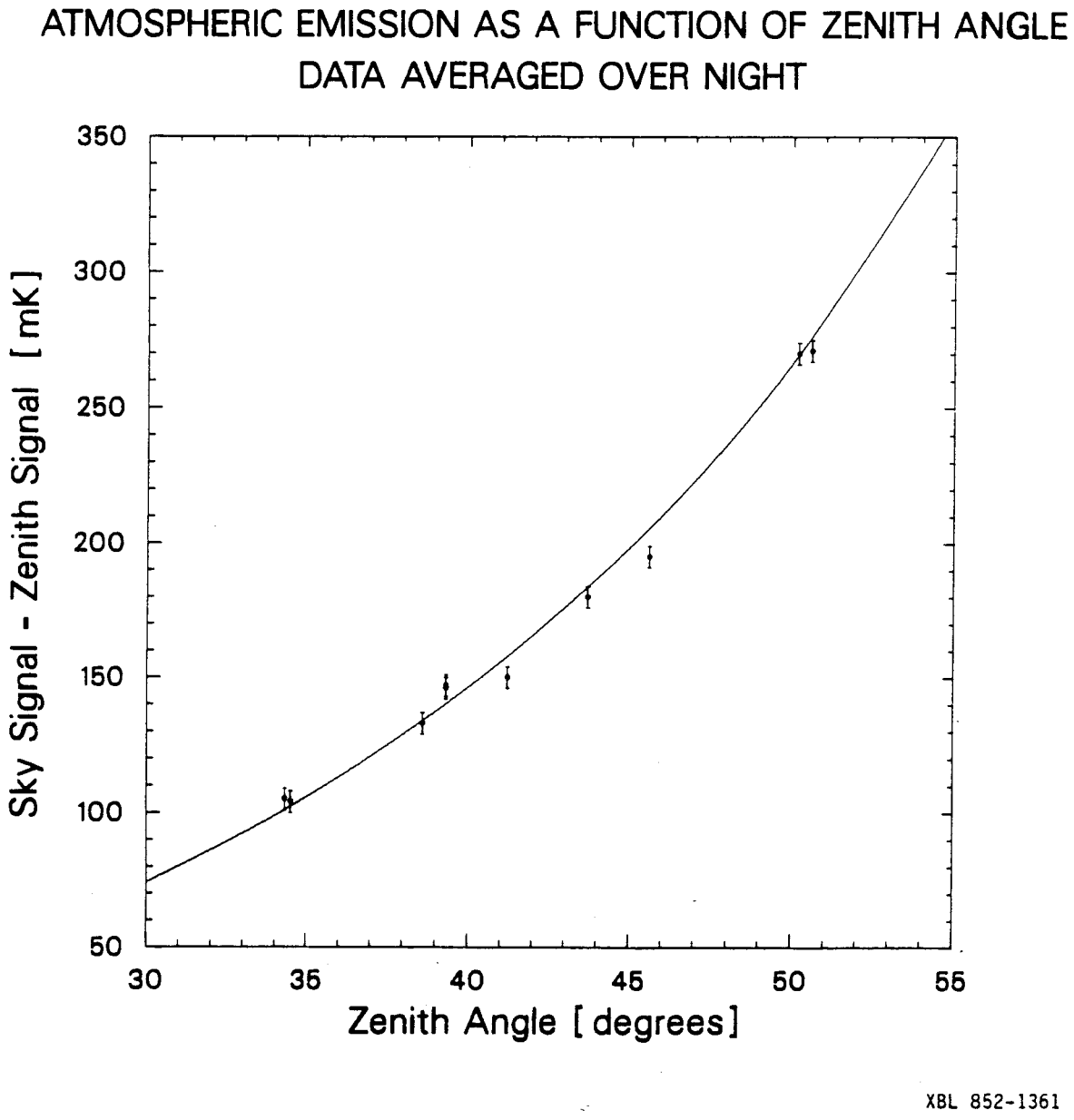

Figure 5 - Atmospheric emission versus zenith angle. The points are the difference between the measured value at angle θ and the zenith. The curve, added to aid the eye, is $(\sec\theta - 1)$ scaled by $T_{A.atm}$. a) Typical values for a single run. b) Values average for one nights data.

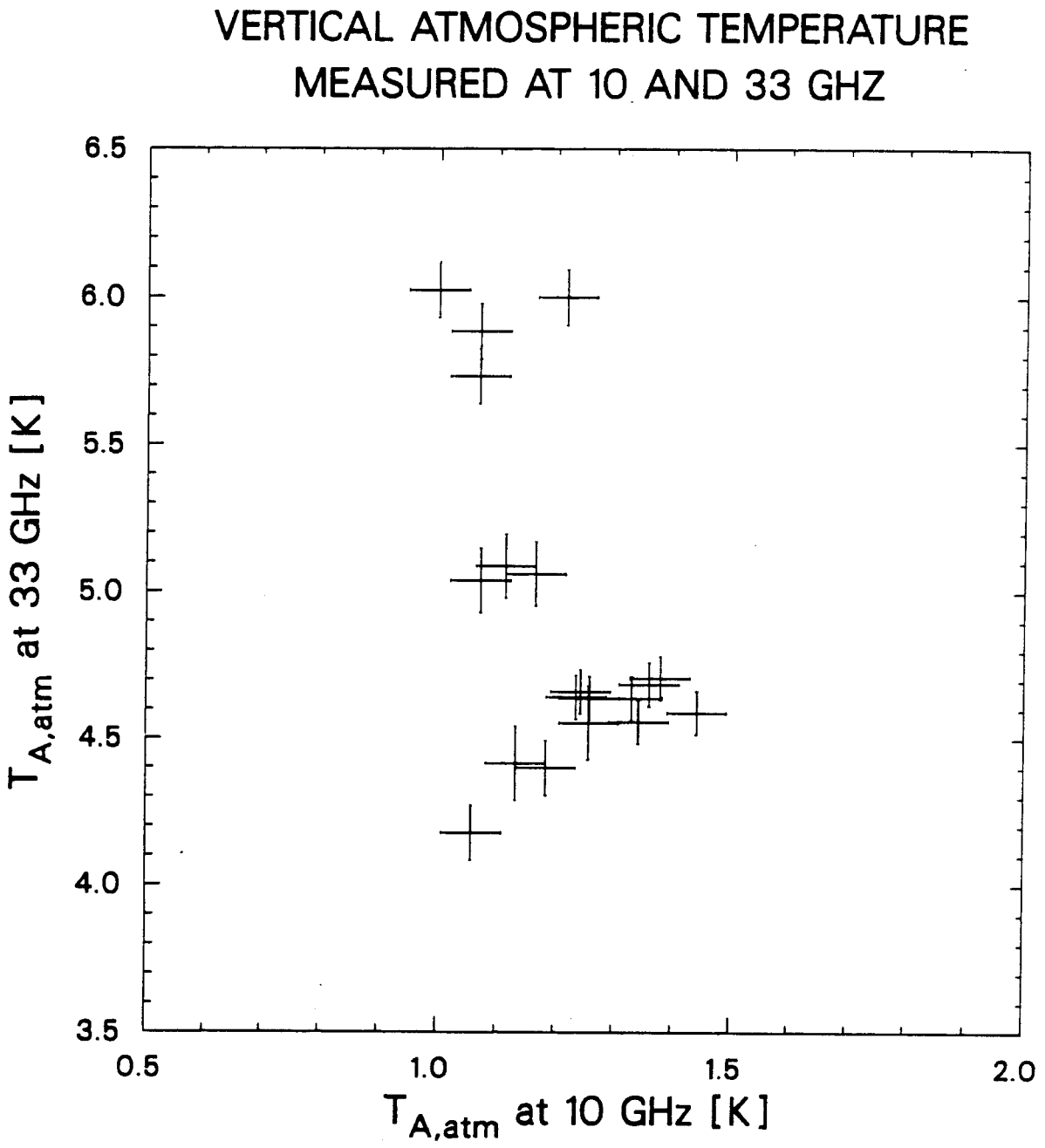

Figure 6a - Vertical atmosphere's temperature at 10 GHz versus that at 33 GHz during 1983

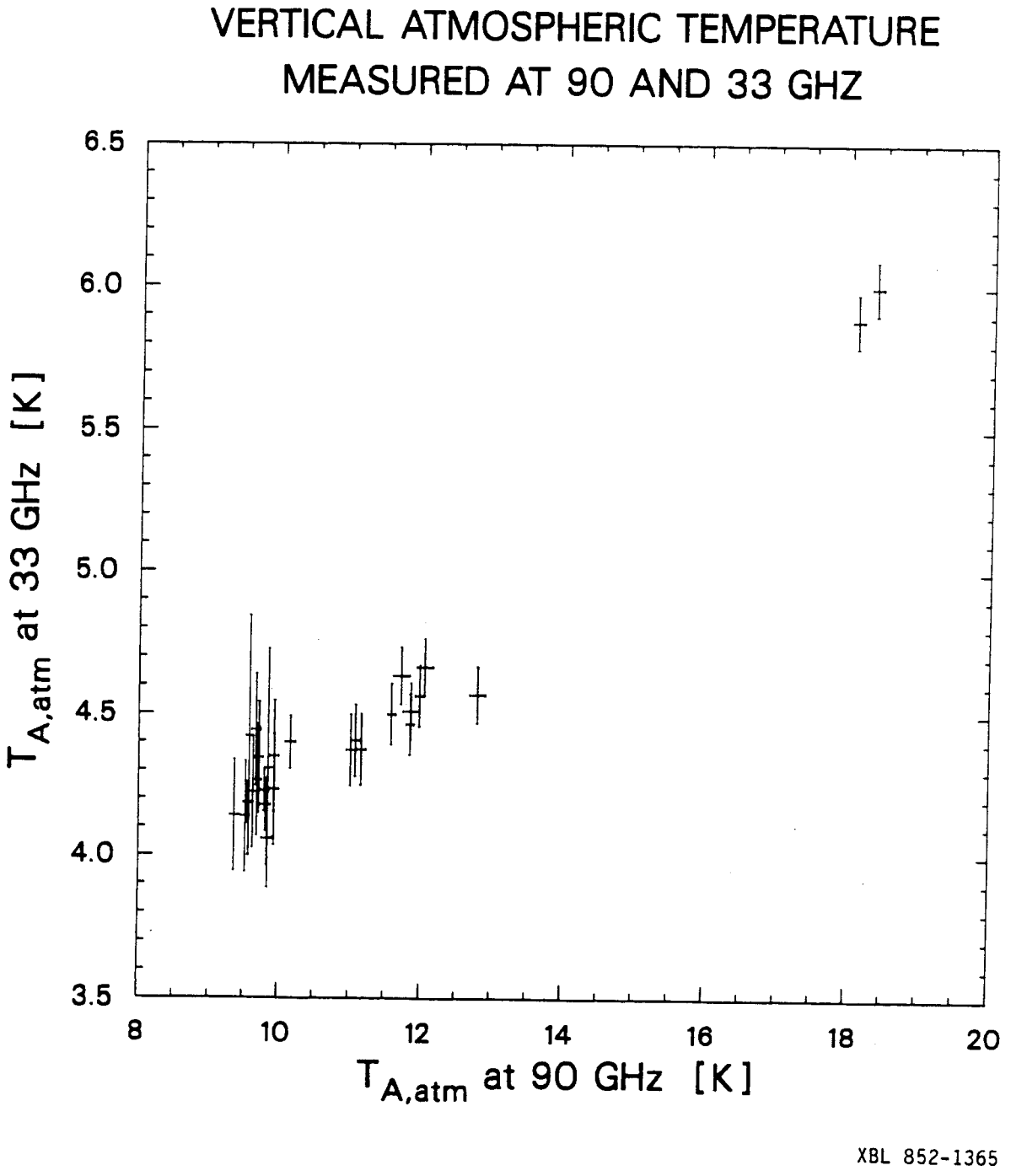

Figure 6b - Vertical atmosphere's temperature at 90 GHz versus that at 33 GHz during 1983

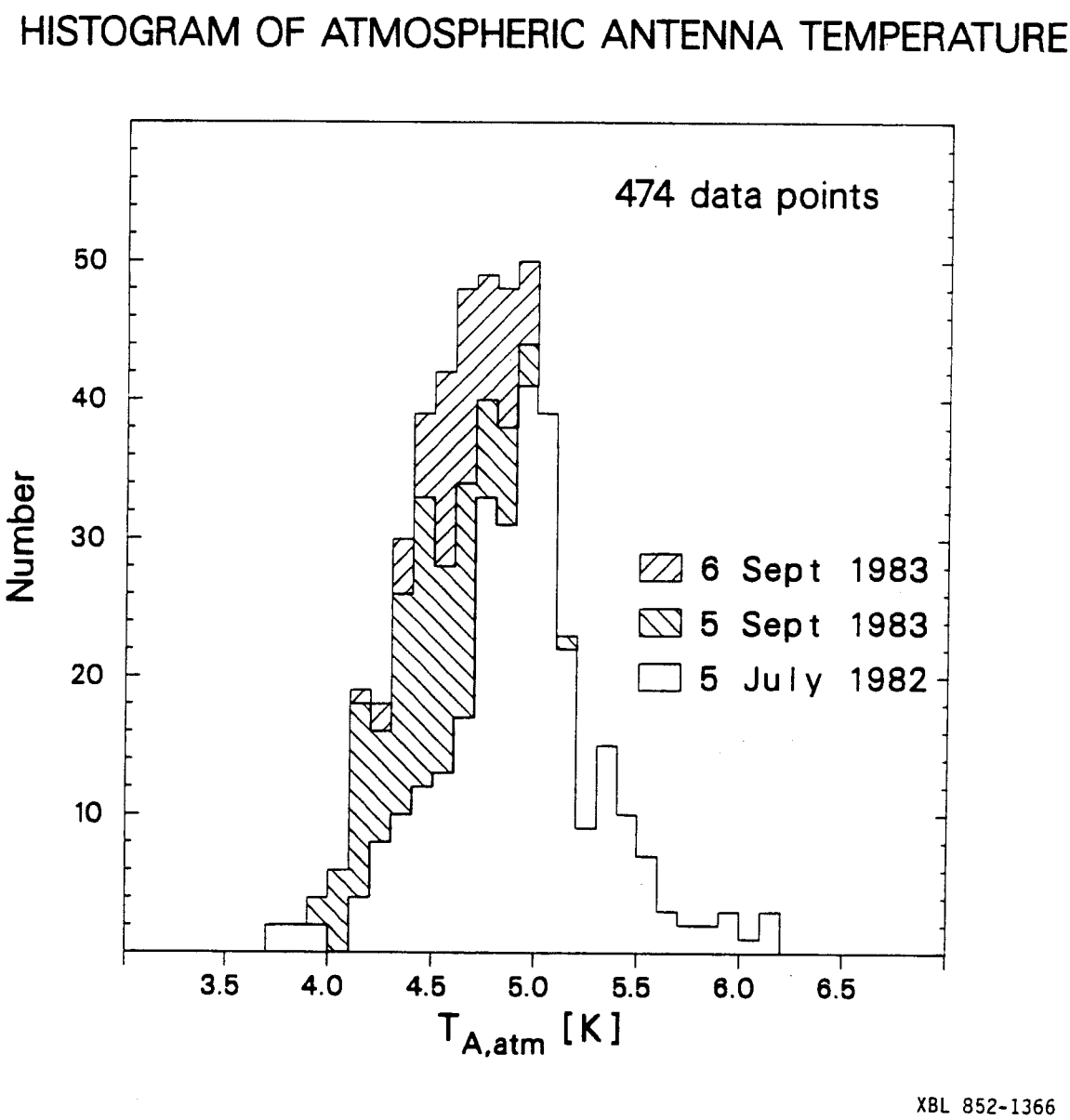

Figure 7 - Histogram of measured atmospheric antenna temperature at vertical

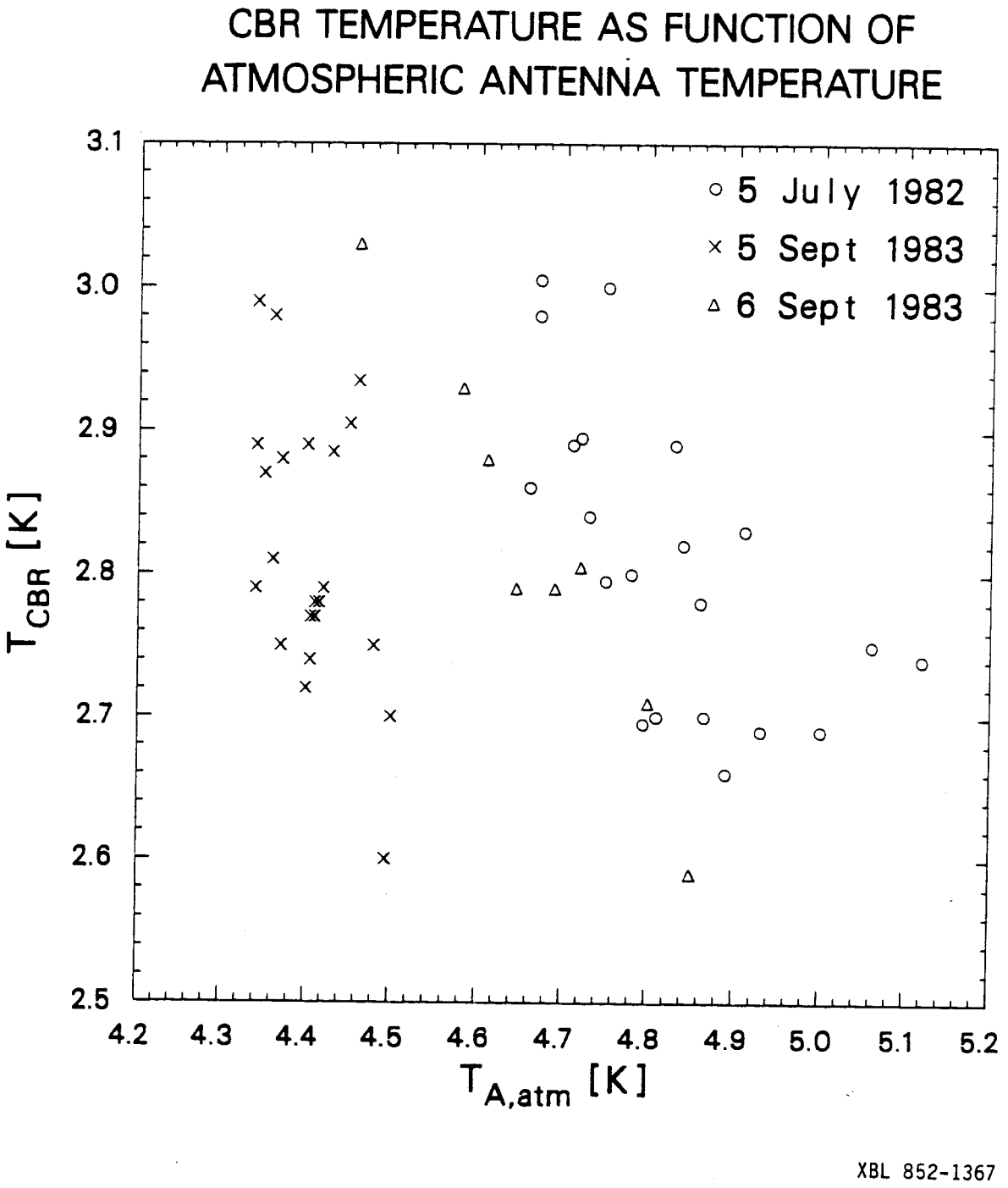

Figure 8 - CBR temperature versus atmospheric antenna temperature. Correlation between the vertical atmosphere's temperature and the measured temperature of the CBR. Errors on $T_{A,atm}$ cause the diagonal scatter of the T_{CBR} data of July 5, 1982 and Sept. 6, 1983.

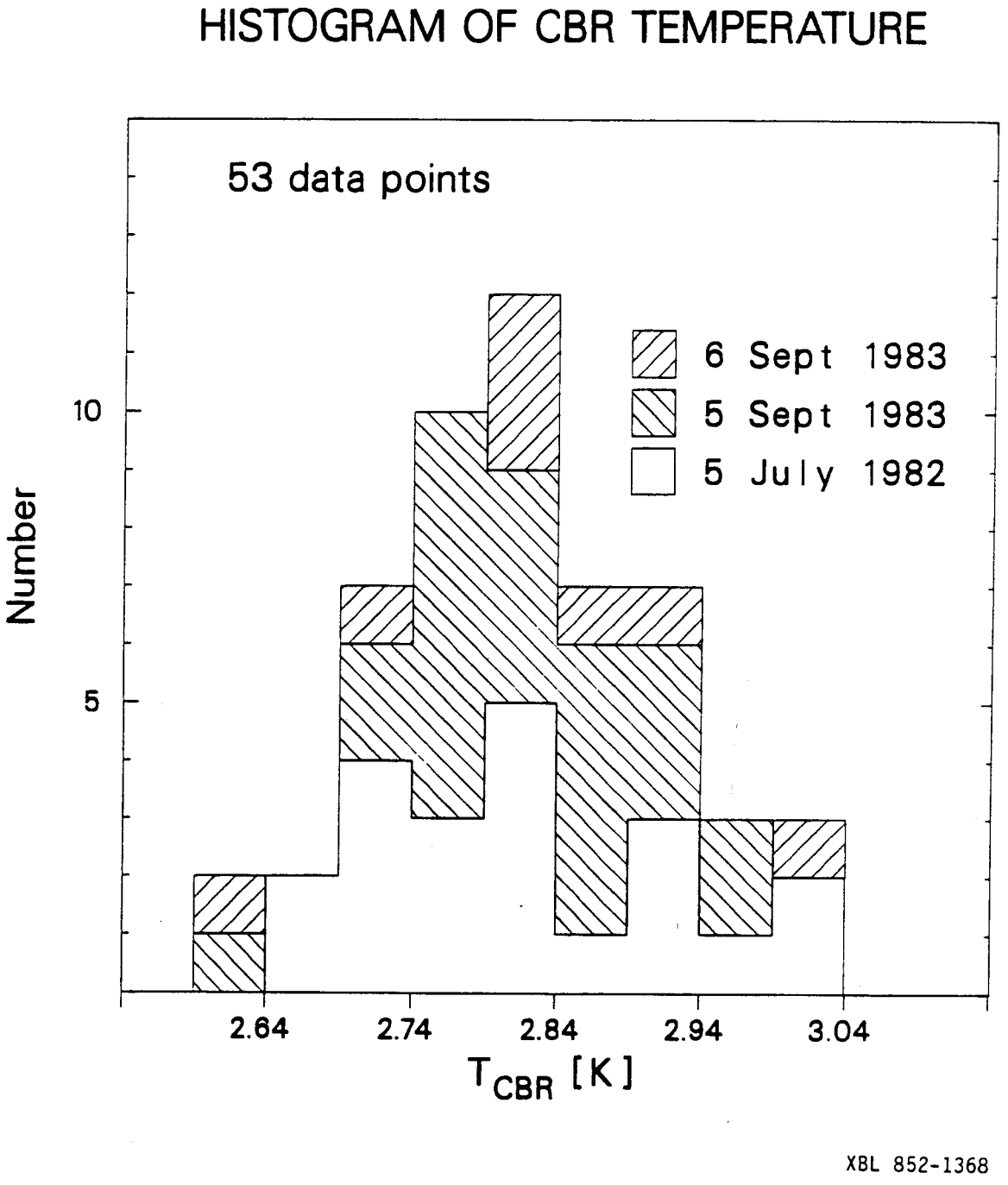

Figure 9 - Histogram of the distribution of the measurements of T_{CBR}. The data have been divided in bins, 50 mK wide, centered around the weighted average.

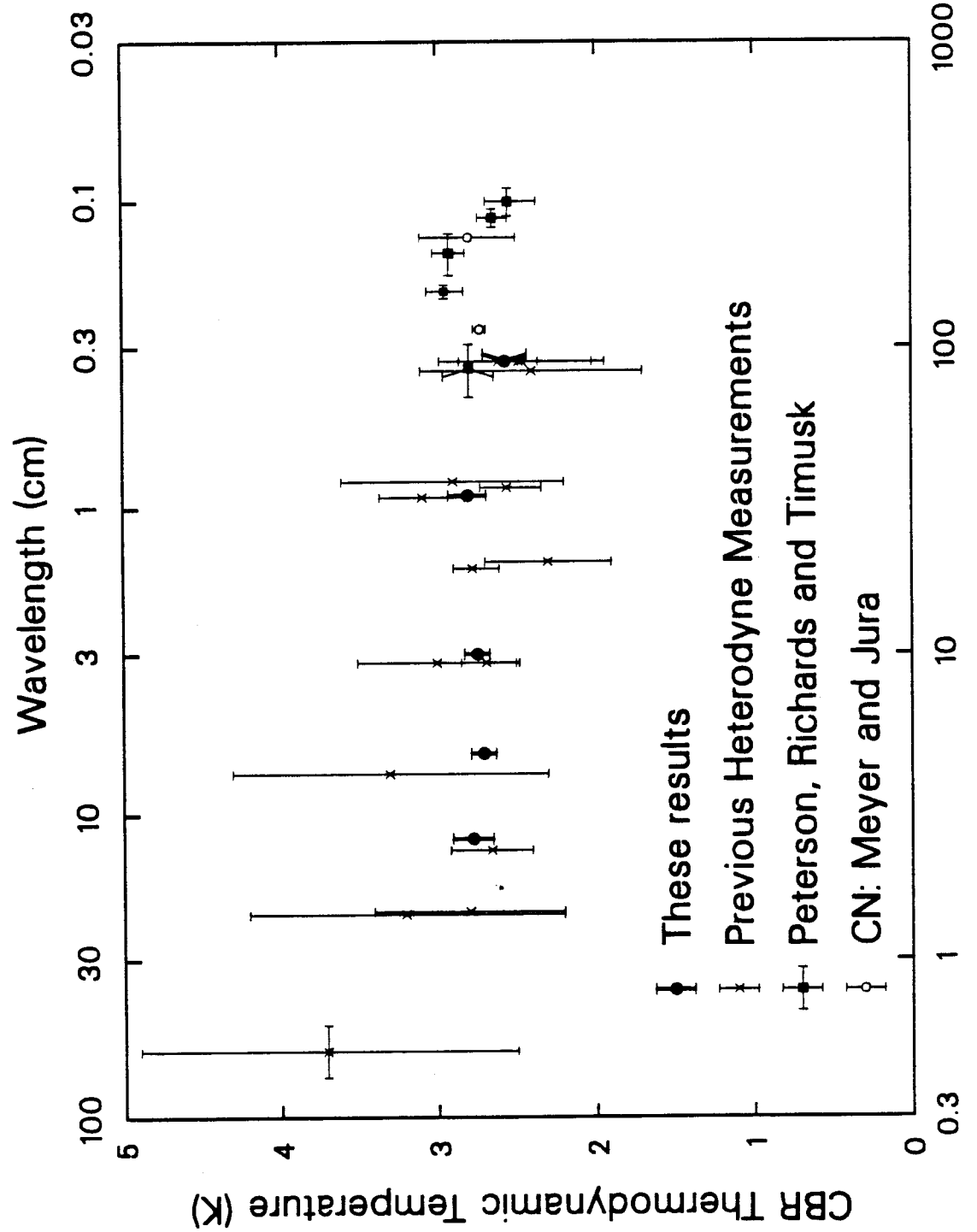

Figure 10 - Previous and present measurements of the thermodynamic temperature of the CBR. All the low frequency data are represented; above 90 GHz only the most recent ones have been plotted.